In presenting the dissertation as a partial fulfillment of the requirements for an advanced degree from the Georgia Institute of Technology, I agree that the Library of the Institute shall make it available for inspection and circulation in accordance with its regulations governing materials of this type. I agree that permission to copy from, or to publish from, this dissertation may be granted by the professor under whose direction it was written, or, in his absence, by the Dean of the Graduate Division when such copying or publication is solely for scholarly purposes and does not involve potential financial gain. It is understood that any copying from, or publication of, this dissertation which involves potential financial gain will not be allowed without written permission.

7/25/68

^{59}Co NMR AND THE OPTICAL ACTIVITY OF SOME AMINE COMPLEXES OF COBALT(III)

A THESIS

Presented to

The Faculty of the Graduate Division

by

Roddie Reagan Judkins

In Partial Fulfillment

of the Requirements for the Degree

Doctor of Philosophy

in the School of Chemistry

Georgia Institute of Technology

March, 1970

^{59}Co NMR AND THE OPTICAL ACTIVITY OF SOME AMINE COMPLEXES OF COBALT(III)

Approved:

Chairman

Date Approved by Chairman: April 2, 1970

ACKNOWLEDGMENTS

This author would sincerely like to express his appreciation to the director of this research, Dr. Donald J. Royer, for his kindness, friendship, and excellent guidance during the course of the research.

Much gratitude is also extended to the members of the reading committee, Dr. Sidney L. Gordon and Dr. Thomas F. Moran, for helpful suggestions concerning the preparation of this manuscript.

Thanks are extended to Dr. Wm. M. Spicer for providing an instructorship during the course of the work, and to the Du Pont Company for fellowship support during a portion of the work.

TABLE OF CONTENTS

LIST OF TABLES

LIST OF FIGURES

LIST OF FIGURES (Continued)

SUMMARY

Preparations and resolutions (into optical isomers) of some high symmetry (C_3 or D_3) *tris*-bidentate amine complexes of cobalt(III) were made. The complex ions studied were $\Lambda(+)_{589}$-*tris*-(ethylenediamine)cobalt (III), $\Lambda(+)_{589}$-*tris*-(*d*-1,2-propanediamine)cobalt(III), and $\Delta(+)_{589}$-*tris*-(1,3-propanediamine)cobalt(III).

The electronic absorption, optical rotatory dispersion, and circular dichroism spectra of the complex ions were obtained. Single crystal electronic absorption and circular dichroism spectra were obtained for compounds containing the complex ions.

The electronic absorption spectra were routinely obtained for determination of concentrations of the solutions. The optical rotatory dispersion spectra were obtained primarily as a test for optical purity on the basis of comparison with published optical rotation values.

The results of the single crystal spectral measurements allowed unequivocal identification of the component bands of the circular dichroism curves. Calculations of the magnitudes of splitting of the trigonal components of the spectra were made on the basis of the solution and single crystal circular dichroism measurements. The method used for the evaluation of the splitting is discussed in Chapter IV.

Magnitudes of the distortions of the complex ions from octahedral symmetry were determined from published X-ray work and the results of solid state nuclear magnetic resonance studies obtained in this work. Qualitative correlations were observed betweeen the distortions deter-

mined by X-ray studies and by nmr methods.

The results of the nmr studies were evaluations of quadrupole coupling constants and asymmetry parameters which give indications of electronic distortions. The quadrupole coupling constants (which indicate the magnitude of distortion along the C_3 axis) varied in the same order as the magnitudes of the trigonal splitting of the circular dichroism curves. That is, the greater the value of the coupling constant, the greater the magnitude of trigonal splitting (see Tables 4 and 7). Thus, apparently the trigonal splitting is due to axial distortion.

The experimental results were compared with predictions made by various theories of the optical activity of complex ions. A theory that was qualitatively correct in terms of the results of this work was a molecular orbital model of Karipides and Piper. This theory is discussed in Chapter II.

The empirical rule for relating the sign of the long wavelength circular dichroism band to the absolute configuration was found to hold in the cases studied here. That is, for the ions studied here, a Λ-type ion had a positive long wavelength component and a Δ-type ion had an negative long wavelength component.

In addition to the complexes mentioned above, the ion, $(+)_{589}$-*tris*-(triethylenetetramine)dicobalt(III) was prepared. Electronic absorption, optical rotatory dispersion, and circular dichroism spectra of this ion were measured. These spectra were very similar to the corresponding spectra for $\Lambda[Co(en)_3]^{3+}$. Nuclear magnetic resonance experiments were performed on single crystals of a nitrate salt of this

ion. The nmr data indicated two unique cobalt nuclei in this salt. The values of the coupling constants for these nuclei were identical and were of the same order of magnitude as the coupling constants for the other ions studied here.

CHAPTER I

INTRODUCTION

In 1812, Biot (1) discovered that quartz crystals rotate the plane of linearly polarized light, and subsequently found (2) that other substances (such as the terpenes and the sugars) possessed the same property. Biot (3) introduced the concept of specific rotation, namely,

$$[\alpha] = \alpha/ldp, \tag{1}$$

where α is the observed rotation in degrees, l is the path length in decimeters, d is the density of the medium and p is the weight fraction of optically active substance.

Fresnel (4) attributed optical rotation to the different refractive indices for left- and right-circularly polarized light,

$$\alpha = (n_l - n_r)\ \pi/\lambda \tag{2}$$

where α is the rotation in radians per unit length, n_l and n_r are, respectively, the refractive indices for left- and right-circularly polarized light, and λ is the wavelength of the incident light.

If the quantity $n_l - n_r$ is not zero at wavelengths where the optically active medium is transparent, then the quantity $\varepsilon_l - \varepsilon_r$ (the difference in extinction coefficients for left and right-circularly polarized light) should have a finite value at frequencies where significant absorption takes place. This phenomenon is known as circular dichroism

and was observed by Haidinger (5) in crystals of amethyst quartz and by Cotton (6) in solutions of copper(II) and chromium(III) (+)-tartrate. This phenomenon became known as the "Cotton effect," and is manifest by differential absorption of left and right-circularly polarized light and by the anomalous dispersion of the optical rotation.

An optically active medium may owe its rotatory power to one or both of two causes: molecular dissymmetry (a term coined by Pasteur to describe molecules that were nonsuperimposable on their mirror images) and macroscopic anisotropy which may be due to the spatial arrangement of the molecules (e.g., crystal lattice) or to the presence of fields (e.g., the Faraday effect). This thesis deals with compounds that owe their optical activity to molecular dissymmetry and throughout the reference to optically active compounds will infer compounds possessing molecular dissymmetry.

Interest here is centered on a particular family of molecules with high symmetry (D_3 or C_3), namely some *tris*-bidentate amine complexes of cobalt(III). These complexes may be classed as essentially octahedral, but their identical ligands consist of three bidentate groups, rather than six identical monodentate groups. Particular complex ions of interest are, $[Co(en)_3]^{+++}$, $[Co(tn)_3]^{+++}$, and $[Co(pn)_3]^{+++}$ whose ligands are, respectively, ethylenediamine, 1,3-propanediamine, and 1,2-propanediamine. The particular interest in these complexes arises because they are the only three members of this family that have had the absolute configurations of their optical isomers established by X-ray methods.

The absorption bands of transition-metal complexes, which lie in the accessible ultraviolet and visible wavelength regions, may be ascribed

to excitations within a restricted group of d electrons associated with the central ion. Generally, regardless of the symmetries of the surrounding ligands, their intensities are quite low. Thus, to a first approximation the $g \leftrightarrow g$ selection rule remains valid for these complexes. When intensities are high, the bands apparently have their origin in charge-transfer and more complex transitions.

For the complexes in question, two bands in the easily accessible region need to be considered. A "typical" absorption spectrum showing these two bands is shown in Figure 1. This particular spectrum is for an aqueous solution containing $[Co(pn)_3]^{+++}$, but the other complexes show quite similar spectra. The longer wavelength bands (around 470 mμ) are ascribed to the transition $^1A_{1g} \rightarrow {}^1T_{1g}$ and the shorter wavelength bands (around 340 mμ) are ascribed to the transition $^1A_{1g} \rightarrow {}^1T_{2g}$. The molar extinction coefficients of both are always less than about 100, so they are assigned to predominantly $d \rightarrow d$ electronic excitations.

The identification of the bands was made on energetic grounds. Calculations by Orgel (7) indicate that the $^1T_{2g}$ state should lie above the $^1T_{1g}$ state. Of the two absorption, bands the $^1A_{1g} \rightarrow {}^1T_{1g}$ band is strongly optically active while the $^1A_{1g} \rightarrow {}^1T_{2g}$ band is weakly optically active. Principal attention here will be given to the strongly rotating, $^1A_{1g} \rightarrow {}^1T_{1g}$, band.

In the presence of a trigonal field, the upper level of each of the transitions, $^1A_{1g} \rightarrow {}^1T_{1g}$ and $^1A_{1g} \rightarrow {}^1T_{2g}$, splits into a doubly degenerate E and a non-degenerate A level. The component bands, $^1A_1 \rightarrow {}^1A_2$ and $^1A_1 \rightarrow {}^1E_a$, of the $^1A_{1g} \rightarrow {}^1T_{1g}$ transition are fairly well resolved in the circular dichroism spectra and are of opposite sign.

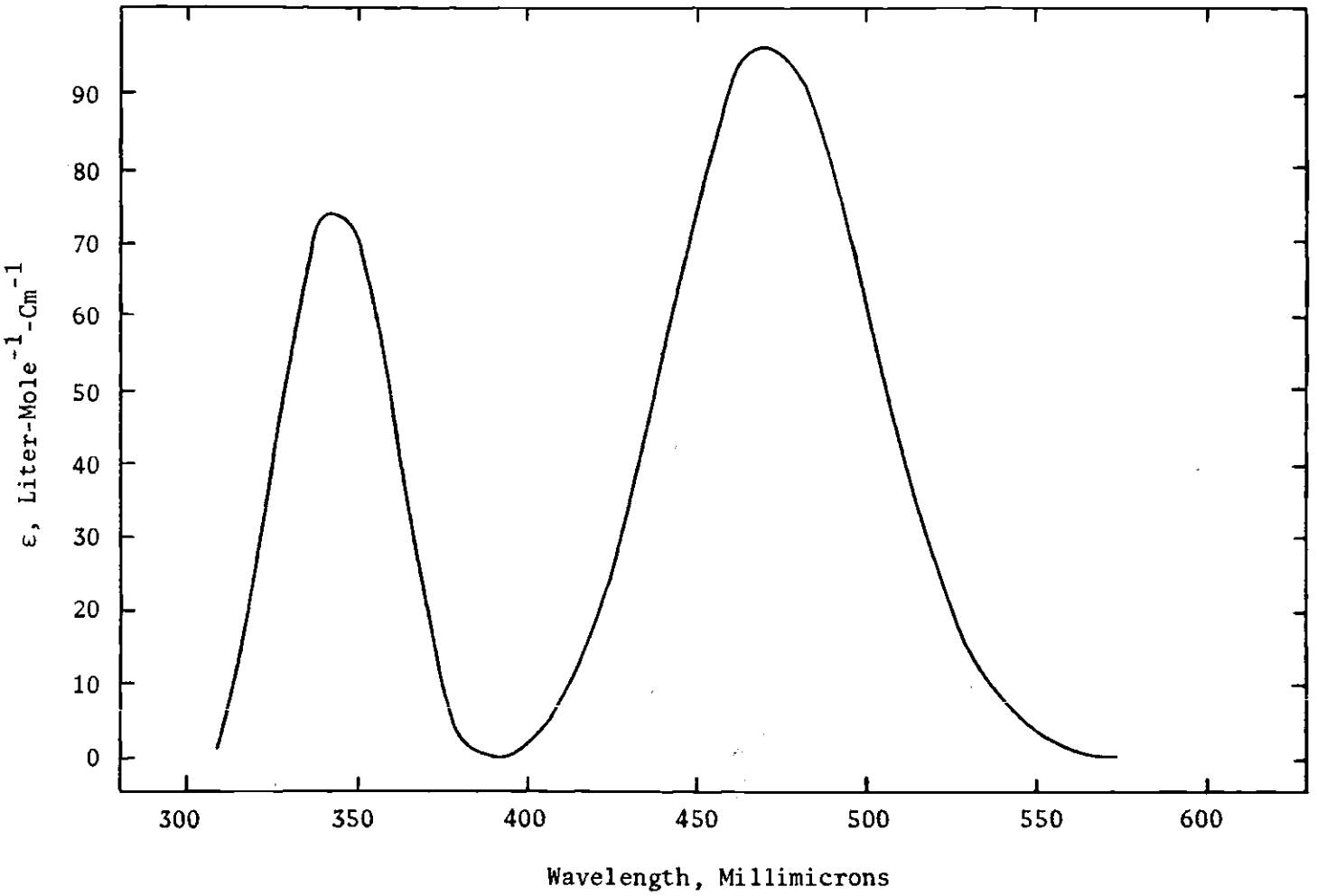

Figure 1. Visible Absorption Spectrum of $[Co(pn)_3]Br_3$; Aqueous Solution

The origin of the optical activity exhibited by complexes of this type has been treated in a number of current theories (8-18). Generally, these theories have attempted to ascribe the optical activity to distortion (nuclear or electronic) of the complex ions from octahedral symmetry. Some of the general features of some of these theories will be discussed in Chapter II, but generally, the goal of these theories has been an explanation of the signs and magnitudes of the trigonal splittings and the optical activities.

The problem of identification of component bands of the circular dichroism (CD) spectra may be solved by propagation of light along the principal (C_3) axis of the complex ion. Due to the selection rules (10) only the *E* components are excited. If a crystal containing the ion in question in a known orientation with respect to the crystallographic axes is available, measurement of the CD with light propagation parallel to the C_3 axis would provide unequivocal identification of the CD bands.

The absolute configurations of three of the complex ions studied here, namely $\Lambda(+)_{589}[Co(en)_3]^{+++}$, $\Lambda(+)_{589}[Co\{(+)\text{-}(pn)_3\}\delta\delta\delta]^{+++}$, and $\Delta(+)_{589}[Co(tn)_3]^{+++}$ have been established by X-ray diffraction studies (19-23) on compounds containing either these ions or their enantiomorphs. The use of the symbols Λ, Δ, δ, and $(+)_\lambda$ corresponds to the recommendations of the Commission on the Nomenclature of Inorganic Chemistry of the International Union of Pure and Applied Chemistry (24). For example, the Δ-type ion presents a right-handed helix when viewed along the C_3 axis (see Figure 2). The symbol, $(+)_\lambda$, refers to the sense of the rotation at the wavelength, λ.

From the X-ray studies, orientations of the complex ions with

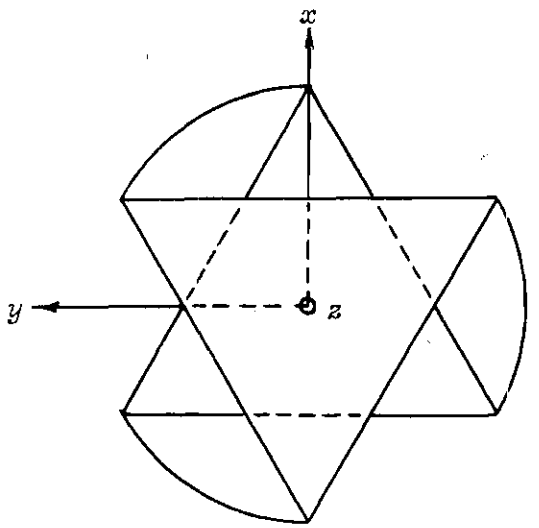

Δ-Isomer

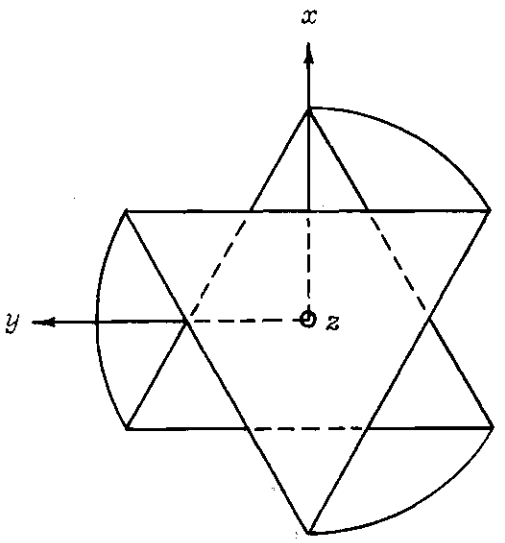

Λ-Isomer

Figure 2. The Optical Isomers of the *Tris*-Bidentate Ions

respect to crystallographic axes were determined. Also, bond lengths and bond angles were determined, and the distortions of the atoms (from octahedral symmetry) were established. That the atomic distortions are not necessarily identical to the electronic distortions has been recognized (16,18). Thus, the X-ray work alone is not sufficient to attempt an explanation of the optical rotatory power on the basis of distortions from octahedral symmetry.

Radio-frequency spectroscopy makes available a number of parameters that may be used to investigate the electron distribution in molecules. These parameters are usually measures of weak interactions occurring between atomic nuclei having magnetic or electrostatic moments and the electrons. Of those parameters measurable in diamagnetic molecules, the best understood is the nuclear electric quadrupole coupling constant. The information provided by the nuclear quadrupole coupling constant is the magnitude of the deviation of the electric-field-gradient, at the nucleus in question, from spherical or cubic symmetry. A second quantity of interest is the asymmetry parameter of the nuclear quadrupole coupling constant tensor which provides a measure of the deviation of the electric-field-gradient from axial symmetry.

A useful method of establishing the electronic asymmetry is by "wide-line" (or solid-state) nuclear magnetic resonance. A theoretical discussion of this technique is given in Chapter II. Also given in Chapter II are methods of relating experimentally observed resonance frequencies to the nuclear electric quadrupole coupling constant and the asymmetry parameter and the orientation of the electric-field-gradient with respect to the polarizing magnetic field.

Generally, this thesis reports the investigation and interpretation of the CD spectra of the complex ions, $\Lambda(+)_{589}[Co(en)_3]^{+++}$, $\Lambda(+)_{589}[Co\{(+)\text{-}(pn)_3\}\delta\delta\delta]^{+++}$, and $\Delta(+)_{589}[Co(tn)_3]^{+++}$ both in aqueous solution and in the solid state. In addition, the investigation of some solid compounds containing these ions by the interpretation of their ^{59}Co radio-frequency absorption spectra (nuclear magnetic resonance spectra) is reported. Particularly, single crystals of $\{[Co(en)_3]Cl_3\}_2 \cdot NaCl \cdot 6H_2O$, $[Co(tn)_3]Cl_3 \cdot 4H_2O$, and $[Co(tn)_3](NO_3)_3$ and a powder of $\Lambda(+)_{589}[Co\{(+)\text{-}(pn)_3\}\delta\delta\delta]Br_3$ were investigated by use of nuclear magnetic resonance.

In addition to the complex ions mentioned above, the ion $[Co_2(trien)_3]^{6+}$ (the ligand is triethylenetetramine) was studied. Apparently, there have been no reported resolutions of this ion into optically active isomers since compounds containing the ion were first reported by Basolo (25). Also, no reported crystal structure determination of a compound containing this ion has been found. However, Busch (26) has suggested a structure for the ion that involves the bridging of three molecules of the tetrafunctional ligand between the two metal atoms in such a way that each ligand is bidentate toward each metal atom. Such a structure would provide the possibility of optically active isomers. Thus, it was of interest to attempt to resolve the ion into optical isomers and to investigate the features of the CD curve and the nmr spectrum of compounds containing this ion.

The resolution of this ion and measurements of the CD and optical rotatory dispersion (ORD) spectra of this ion in aqueous solution are reported herein. Also, ^{59}Co nmr spectra of this ion in single crystals of $[Co_2(trien)_3](NO_3)_6 \cdot 6H_2O$ are reported.

CHAPTER II

THEORY

Theories of Optical Activity

The quantum mechanical expression for optical rotation was derived by Rosenfeld (27). As specified by Rosenfeld (27) and Condon (28), the contribution of an electronic transition from state a to state b to the total rotation is determined by the rotational strength, R_{ba}, defined as the imaginary part of the scalar product of the electric and the magnetic dipole moments associated with the transition,

$$R_{ba} = \mathrm{Im}\{(a|\mathrm{P}|b)\cdot(b|\mathrm{M}|a)\}, \tag{3}$$

where P and M are, respectively, the electric and the magnetic dipole operators. The magnetic moment operator is complex,

$$\mathrm{M} = (-ieh/4\pi m_e c)d/d\phi, \tag{4}$$

where e and m_e are, respectively, the charge and the mass of the electron, h is Planck's constant, c is the velocity of light, and ϕ is the angle of rotation about a given axis. The electric moment operator is real,

$$\mathrm{P} = e\mathrm{r}, \tag{5}$$

where r is a vector defining the position of the electron.

For a dissymmetric molecule, Hückel (29) has shown that Eq. [3] can be simplified to the form,

$$R_{ba} = \mu_e \mu_m \cos\theta; \tag{6}$$

where μ_e and μ_m are, respectively, the electric dipole and magnetic dipole transition moments defined as

$$\mu_e = \int (a|P|b)d\tau \qquad \mu_m = \int (b|M|a)d\tau \tag{7}$$

and θ is the angle between the directions of the two moments.

The general relation between the rotatory strength and the area under the circular dichroism (CD) curves as given by Moffitt and Moscowitz (30) is,

$$R_{ba} = \frac{3hc10^3 ln10}{32\pi^3 N} \int \frac{\varepsilon_l - \varepsilon_r}{\nu} d\nu \tag{8}$$

where the constants have their usual significance, $\varepsilon_l - \varepsilon_r$ is the differential molar decadic extinction coefficient, i.e., the difference in the molar decadic extinction coefficients for left and right-circularly polarized light at the frequency ν. For a Gaussian dichroism band, Eq. [8] yields,

$$R_{ba} \simeq 24.5 \times 10^{-40} (\varepsilon_l - \varepsilon_r)_{max} \frac{\Delta\nu_{1/2}}{\nu_o} \tag{9}$$

where $(\varepsilon_l - \varepsilon_r)_{max}$ is the maximum of the CD curve, ν_o is the frequency at this maximum, and $\Delta\nu_{1/2}$ is the half-width, i.e., the width of the band at half-maximum differential absorption. The resulting rotational strength, R_{ba}, will be in c.g.s. units. Thus, the rotational strength is related to the CD curve in a fashion similar to the way that the

dipole strength, D, is related to the absorption curve, i.e.,

$$D = \frac{3hc\ 10^3\ ln\ 10}{8\pi^3 N} \int (\varepsilon/\nu) d\nu, \qquad (10)$$

From Eq. [3], the condition for optical rotation is that the imaginary part of the scalar product of the magnetic and electric dipole moments be different from zero for the transition $a \rightarrow b$. If the molecule has second-order symmetry elements, i.e., either a plane or center of symmetry or a mirror axis, the scalar product of these two elements cannot be different from zero. If any of these symmetry elements exist, there are no two states for which the scalar product of the electric and magnetic dipole matrix elements does not vanish.

Several models (8-18) have been advanced for the origin of optical activity exhibited by dissymmetric transition metal complexes in the wavelength region of their absorption bands. It is not the intent here to give a detailed derivation of these theoretical models. Instead, it is desired to test the predictions of these theoretical models by use of the present experimental results.

The Coupled Oscillator Model

Kuhn and Bein (8) used a coupled oscillator model for the first theoretical treatment of the rotatory dispersion of octahedral *tris*-bidentate complexes.

The central atom was represented by an isotropic harmonic oscillator of frequency ν_o and the ligands were represented by three linear oscillators of frequency ν_1 ($\nu_1 > \nu_o$). Introduction of coupling forces between the central atom and the ligands and between ligands resulted in

six oscillations. Three of these oscillations had characteristic frequencies near ν_1 and three had characteristic frequencies near ν_o. Two of the oscillations near ν_o were of identical frequency and of symmetry type *E* and one was of symmetry type *A*. The components of the *E* oscillations were polarized perpendicular to the trigonal axis and the *A* oscillation was polarized parallel to the trigonal axis. The oscillations would be optically active and the contribution to the optical activity of the *A* and *E* oscillations could be of opposite or identical sign.

For *A* and *E* contributions to rotatory strength of identical sign, the relation between the absolute configuration of the ion and the predicted sign of its rotatory strength is unambigious. That is, ions of the same absolute configuration would have rotatory strengths of the same sign. However, if the *A* and *E* contributions to rotatory strength are of opposite signs, the relation is unambigious only if the observed band can be identified. That is, ions of the same absolute configuration would have component bands of the same sign, but an identification of these component bands would have to be made in order to relate the signs of the bands to the absolute configuration.

The Harmonic Oscillator Model

Jones and Eyring (9) used the anisotropic, asymmetric, harmonic oscillator model of Condon, Altar, and Eyring (31) to predict absolute configurations of optically active molecules from optical rotatory dispersion (ORD) data.

The potential function used was,

$$V = 1/2\ K_1x^2 + 1/2\ K_2y^2 + 1/2\ K_3z^2 + Axyz \qquad (11)$$

where x,y, and z are three orthogonal coordinates. The anistropic condition is satisfied if $K_1 \neq K_2 \neq K_3$. The term in A is what produces the necessary asymmetry.

The result of this model was that the rotation is proportional to the parameter A, the differences between the frequencies of the transitions in the various directions, and the quantum numbers of the initial state. In this model, the sign of the rotation follows the sign of A. Jones and Eyring showed that for a Δ configuration, the rotation would be negative.

This method ascribes a rotatory power of the same sign to the A and E components. Also, in the model of Condon, Altar, and Eyring (31), if any two of the electronic transitions directed along the coordinate axes of the molecule have the same frequency, as in the case of the degenerate E component, the rotatory power vanishes.

The Ionic Model

Moffitt (10) was the first to attempt an interpretation of the optical activity of octahedral *tris*-bidentate complexes in terms of the crystal field theory. An especially important achievement of this treatment was the explanation of the fact that one of the two visible absorption bands observed in *tris*-(ethylenediamine)cobalt(III) should be strongly optically active whereas the second should be only weakly optically active. For cobalt(III) in an octahedral site, the two bands are ascribed to the two transitions, $^1A_{1g} \rightarrow {}^1T_{1g}$ and $^1A_{1g} \rightarrow {}^1T_{2g}$, in order of increasing energy. The transition, $^1A_{1g} \rightarrow {}^1T_{2g}$ is magnetically forbidden and from Eq. [3] should be optically inactive. The transition, $^1A_{1g} \rightarrow {}^1T_{1g}$, is magnetically allowed and thus could be optically active. In

Moffitt's detailed treatment of the optical activity of the first band, an error of calculation was made and to the approximation made by Moffitt this band is also optically inactive. This error was pointed out by Sugano (32).

Hamer (11), Piper and Karipides (12), Poulet (13), and Shinada (14) have taken the basic features of Moffitt's approach and extended them. The first three treatments are very similar in that rotatory power is introduced through a perturbation of the octahedral field by a trigonal potential of odd parity. With this approach, the absorption that corresponds to $^1A_{1g} \rightarrow {}^1T_{1g}$ is split into two overlapping optically active absorption bands, i.e., the transitions, $^1A_1 \rightarrow {}^1A_2$ and $^1A_1 \rightarrow {}^1E_a$. In terms of the symmetries of the electronic states in dihedral complexes, the selection rules for the electronic transitions are

$$\begin{aligned} A_1 &\leftrightarrow A_2 \qquad (\parallel) \\ A_{1,2} &\leftrightarrow E \qquad (\perp) \\ E &\leftrightarrow E \qquad (\parallel, \perp) \end{aligned} \tag{12}$$

the moments being polarized parallel ($\parallel$) or perpendicular ($\perp$) to the principal (C_3) axis of the chelated complex (see Figure 2). Furthermore, these overlapping bands should be of equal magnitude and opposite sign in the CD spectrum.

In the ionic model of Piper and Karipides (12), the assumption was made that the *3d* orbitals were mixed with the *4p* orbitals in the ungerade trigonal field. This was the assumption made by Moffitt (10); however, Piper and Karipides considered the effect of trigonal splittings, and this model gave a net rotation. According to this model, angular dis-

tortions give rise to trigonal field splittings and to nonvanishing rotational strengths. For example, distortion along axes parallel to the z-axis (see Figure 2) from the polar angle in an octahedron (54.7°) gives rise to a nonvanishing trigonal field splitting. Azimuthal distortion (a twist of the trigonal planes about the z-axis of Figure 2), according to this model, gives rise to a nonvanishing rotational strength.

The sign of the potential in the ionic model is dependent on the sign of a constant coefficient term,

$$ez\sqrt{(2\pi)}\ (3/7)\sqrt{(35/2)}\sin^3\alpha\ \sin\delta \qquad (13)$$

where z is the ligand charge, α is the polar angle (the angle between the C_3 axis of the complex ion and the central atom-ligating atom direction), and δ is one-half the change of the azimuthal angle from the octahedral value of 60°. The azimuthal angle is the angle formed by the projection of the N-Co-N angle of a chelate ring on the xy plane. δ is defined as positive for contraction and negative for expansion of the azimuthal angle for a Δ-molecule and the signs are reversed for a Λ-molecule.

The sign of the rotational strength of the nondegenerate component depends on the sign of the constant part of the potential. Thus, the sign of the rotational strength of the nondegenerate component (A_2) will depend on the sign of δ since α will not be very different from 54.7°. In the ionic model of Piper and Karipides, this sign is determined by the sign of the quantity, vq/ε, where ε is the negative of the excitation energy for the transition, $nd\rightarrow(n+1)p$, q is taken to be the length of the transition moment, and v is a unit that contains the con-

stant and radial parts of the trigonal field potential. According to Piper and Karipides, v and q will have the same sign.

Specifically, Piper and Karipides predicted that for a Λ-type ion with azimuthal expansion, the A_2 component should be positively rotating. Furthermore, if this type ion had an expansion of the polar angle (a compression of the octahedron along the C_3 axis) their prediction is that the trigonal splitting should be negative, i.e., $\nu_E - \nu_A < 0$.

The Molecular Orbital Model

Two molecular orbital models relating to optical activity will be presented here. The first is the model of Karipides and Piper (15) and the second is the model of Liehr (16).

In the Karipides and Piper model, the matrices of the electric moment, ep, and of the magnetic moment, $(e/2m_e c)\vec{m}$, for the one-electron transition, $t_2 \rightarrow e$, are expressed in terms of empirical parameters, q_o, q_1, and q_2, which are taken to be the lengths of the transition moments. The one-electron rotational strengths for a $t_2 \rightarrow e$ transition in terms of these parameters are,

$$\begin{aligned} {}^1A_1 \rightarrow {}^1A_2 \qquad & R = 4\sqrt{2}mq_1 he^2/(2m_e c) \\ {}^1A_1 \rightarrow {}^1E_a \qquad & R = 4\sqrt{2}m(q_o - q_2). \end{aligned} \tag{14}$$

The dipole strengths of the transitions in terms of these parameters are,

$$\begin{aligned} {}^1A_1 \rightarrow {}^1A_2 \qquad & D = 4q_1^2 e^2 \\ {}^1A_1 \rightarrow {}^1E_a \qquad & D = (q_o - q_2)^2 e^2 \\ {}^1A_1 \rightarrow {}^1E_b \qquad & D = (q_o + q_2)^2 e^2 \end{aligned} \tag{15}$$

The parameters, q_o, q_1, and q_2, may be obtained from integrated band intensities, I_{1g} and I_{2g}, of the experimental solution absorption bands, T_{1g} and T_{2g}, respectively, and hypothetical integrated band intensities, I_π and I_σ, of oriented molecules in solution with the light polarized respectively, parallel and perpendicular to the molecular C_3 axis. Assumptions were made that the polarization ratio, $I_\parallel/I_\perp$, in the crystal would apply to the solution as well, and that all the intensity of the T_{2g} band was due to the E_b component. The resulting relationships between the hypothetical integrated band intensities of oriented molecules in solution and the experimental solution absorption bands are,

$$\begin{aligned} I_\pi(T_{1g}) &= [1/3 + 2/3(I_\perp/I_\parallel)]^{-1} I_{1g}, \\ I_\sigma(T_{1g}) &= [1/3(I_\parallel/I_\perp) + 2/3]^{-1} I_{1g}, \\ I_\sigma(T_{2g}) &= 3/2\, I_{2g}. \end{aligned} \tag{16}$$

The q's were then related to the integrated band intensities by the relation.

$$\int (\varepsilon/\nu)d\nu = \frac{8\pi^3 e^2 N}{2303\, hc} \cos^2\alpha |x_{nm}|^2, \tag{17}$$

where α is the angle that the plane of polarization makes with the transition moment, and $|x_{nm}|^2$ represents q_1^2, $(q_o-q_2)^2$, and $(q_o+q_2)^2$ for the bands, A_a, E_a, and E_b, respectively. All other symbols have their usual significance.

The determination of the sign of R in connection with the absolute configuration is summarized in the following discussion. An increase in the polar angle (from 54.7°) results in a negative value of the trigonal splitting, i.e., $\nu_E-\nu_A<0$, and a decrease in the polar angle results in a

positive value of the trigonal splitting. Azimuthal expansion in a Λ type configuration leads to positive q values and azimuthal contraction leads to negative q values. Thus, azimuthal expansion coupled with an increase in the polar angle results in an A_2 component of negative rotatory power and an E_a component of positive rotatory power.

Liehr (16) has suggested a model in which optical activity results from a mismatch, by an angle of cant, α, of the metal and ligand orbitals. In this model, the coordinated nitrogen atoms are located on the regular octahedral axes, and α is the angle between the axes of the overlapping orbitals from the central and ligand atoms.

Liehr's expressions for the rotational strengths for the transitions of interest here are

$$\begin{aligned} {}^1A_1 \rightarrow {}^1A_2 \qquad & R = 4r_1 m_1 \\ {}^1A_1 \rightarrow {}^1E_a \qquad & R = 2(r_o + r_2)(m_o + m_2), \\ {}^1A_1 \rightarrow {}^1A_1 \qquad & R \equiv 0 \\ {}^1A_1 \rightarrow {}^1E_b \qquad & R = 2(r_o - r_2)(m_o - m_2), \end{aligned} \tag{18}$$

where

$$\begin{aligned} r_o &= e/2\eta\sqrt{3/2}k_p \sin\alpha(\sqrt{3}K_{4A3} + K_{7A3})N_{a1(t)}N_{e(e)}, \\ r_1 &= e/2\xi\sqrt{3/2}k_p \sin\alpha(2K_{7A3})N_{e(t)}N_{e(e)}, \\ r_2 &= e/2\xi\sqrt{3/2}k_p \sin\alpha(\sqrt{3}K_{4A3} - K_{7A3})N_{e(t)}N_{e(e)}, \\ m_o &= \sqrt{2}\mu_B N_{a1(t)}N_{e(e)}, \\ \text{and} \quad m_1 &= m_2 = \sqrt{2}\mu_B N_{e(t)}N_{e(e)}. \end{aligned} \tag{19}$$

In Eqs. [19], α is the angle of cant, k_s and k_p are, respectively, the ligand σ bond $2s$ and $2p$-like content, ξ and η are ligand-metal σ, π-mixture parameters, the N's are normalization constants for the indicated orbitals and the quantities K_{nAj} are localized ligand-metal integrals which estimate the localized electric transition dipole moment in the metal-ligating atom direction.

The dependence of the rotational strength on the local orbital mismatch parameter, α, through $\sin\alpha$ indicates that as α goes to zero and through it, the rotation will likewise go to zero, and after α has passed through zero, the rotation will re-emerge with unchanged sign. Thus, in Liehr's model, the sign of the rotational strengths of the *tris*-(diamine) complexes should be determined by the chirality (handedness) of the complex and be independent of the angle of cant, α. According to Karipides' and Piper's model, the sign of the rotational strength is independent of the chirality and determined instead by the displacement of the coordinated atoms from the apices of the regular octahedron.

McCaffery and Mason (17) have proposed a model in which the metal ion transitions acquire a rotational strength by mixing with ligand transitions having electric moments directed perpendicular to the planes of the chelate rings. They suggested that dihedral d^6 complexes have the Λ configuration if the spin-allowed transition of lowest energy has an E component with a positive rotatory power. Their model predicts independence of the sign of the rotational strength on the N-Co-N bond angle.

Nuclear Magnetic Dipole and Nuclear Electric Quadrupole Interactions in Solids

The basic theory of nuclear magnetic dipole and nuclear electric quadrupole interactions in solids has been treated elsewhere (33-39). Emphasis here will be placed on the results of the theory rather than a detailed derivation of the theory.

The principal result of the investigations mentioned above has been the derivation of matrix elements of the interactions of a nuclear magnetic dipole with a magnetic field and a nuclear electric quadrupole with an electric field. Usually, perturbation techniques have been used to relate experimentally observed resonance frequencies to the nuclear electric quadrupole coupling constant, e^2Qq/h, and the asymmetry parameter, η, which describe the shape of the electric field, and the orientation of the electric field gradient with respect to the external magnetic field.

Brown (37) and Parker (40) wrote closed expressions that related the experimental resonance frequencies and the desired parameters by making use of the relationship between the moments of the energy level and the coefficients of the secular equation.

The energy levels, F_i, are expressed in frequency units and the reference level from which they are measured is fixed by requiring that the sum of the energies be zero, i.e.,

$$\Sigma F_i = 0, \; i = 1, 2, 3, \ldots, 2I + 1 \tag{20}$$

For example, for $I = 7/2$, the number of energy levels is eight. The energy levels are calculated from the experimental frequency data by

utilization of Eq. [20] and the relation between the frequencies, ν_i, and the energy levels, namely,

$$\nu_i = F_{i+1} - F_i. \tag{21}$$

The ν_i and the F_i are labeled in order of increasing (or decreasing) magnitude. The expressions,

$$\begin{aligned}
F_1 &= 1/8(-7\nu_1-6\nu_2-5\nu_3-4\nu_4-3\nu_5-2\nu_6-\nu_7),\\
F_2 &= 1/8(\nu_1-6\nu_2-5\nu_3-4\nu_4-3\nu_5-2\nu_6-\nu_7),\\
F_3 &= 1/8(\nu_1+2\nu_2-5\nu_3-4\nu_4-3\nu_5-2\nu_6-\nu_7),\\
F_4 &= 1/8(\nu_1+2\nu_2+3\nu_3-4\nu_4-3\nu_5-2\nu_6-\nu_7),\\
F_5 &= 1/8(\nu_1+2\nu_2+3\nu_3+4\nu_4-3\nu_5-2\nu_6-\nu_7),\\
F_6 &= 1/8(\nu_1+2\nu_2+3\nu_3+4\nu_4+5\nu_5-2\nu_6-\nu_7),\\
F_7 &= 1/8(\nu_1+2\nu_2+3\nu_3+4\nu_4+5\nu_5+6\nu_6-\nu_7),\\
F_8 &= 1/8(\nu_1+2\nu_2+3\nu_3+4\nu_4+5\nu_5+6\nu_6+7\nu_7),
\end{aligned} \tag{22}$$

satisfy both Eqs. [20] and [21]. Inversion of the energy level diagram does not alter the validity of the relations; thus, the absolute signs of the F_i are ambigious and may be determined only with additional information regarding the signs of μH_o and e^2Qq/h.

From the experimentally determined F_i, the secular polynomial may be formed as,

$$(F-F_1)(F-F_2)(F-F_3)\ \ldots\ (F-F_n) = 0, \tag{23}$$

where $n = 2I + 1$ is the multiplicity. Equation [23] may be written as

$$F^n+a_1F^{n-1}+a_2F^{n-2}+a_3F^{n-3}+\ldots +a_n = 0, \tag{24}$$

where,

$$\begin{aligned} a_1 &= -\Sigma F_i, \\ a_2 &= \Sigma F_i F_j \qquad i<j \\ a_3 &= -\Sigma F_i F_j F_k \qquad i<j<k, \\ &\text{etc.} \end{aligned} \tag{25}$$

The stipulation that $i<j<k$ is made to avoid duplication of the sums.

For convenience the sums of the powers of the roots are used,

$$\begin{aligned} S_1 &= \Sigma F_i = -a_1 = 0, \\ S_2 &= \Sigma F_i^2 = -2a_2, \\ S_3 &= \Sigma F_i^3 = -3a_3. \end{aligned} \tag{26}$$

Higher powers of the F_i are omitted since S_1, S_2, and S_3 provide sufficient information in most cases.

The total interaction energy, W, of the nucleus with the surrounding magnetic and electric fields is W^d+W^q, where W^d is the magnetic dipole interaction energy and W^q is the electric quadrupole interaction energy. The matrix elements for the total interaction energy are,

$$\begin{aligned} W_{m,m} &= -m\nu_o \cos\theta + 1/6[3m^2-I(I+1)]C_3 \\ W_{m,m+1} &= -1/2[(I-m)(I+m+1)]^{1/2}\nu_o \sin\theta\, e^{i\phi}, \\ W_{m+1,m} &= W^*_{m,m+1} \\ W_{m,m+2} &= 1/12[(I-m)(I+m+1)(I-m-1)(I+m+2)]^{1/2}\eta C_3, \\ W_{m+2,m} &= W_{m,m+2} \end{aligned} \tag{27}$$

The secular determinant,

$$(-1)^n |W_{ij} - F\delta_{ij}| = 0, \tag{28}$$

on expansion reduces to,

$$F^n + a_1 F^{n-1} + a_2 F^{n-2} + \ldots + a_n = 0. \tag{29}$$

The coefficient of F^{n-1} in Eq. [29] is given by the negative of the sum of the diagonal elements of the secular determinant. Therefore,

$$a_1 = -\Sigma W_{m,m} = (\nu_o \cos\theta)\, m + 1/6\, C_3 \Sigma\{3m^2 - I(I+1)\}, \tag{30}$$

where $m = -I, -I+1, \ldots, +I$.

With the sums extending over all allowed values of m, Eq. [30] yields,

$$a_1 = 0, \tag{31}$$

and from Eq. [26],

$$\Sigma F_i = -a_1 = 0. \tag{32}$$

The coefficient of F^{n-2} is given by the sum of the series of 2 x 2 minors along the diagonal of the secular determinant. Brown's (37) result for this calculation is,

$$a_2 = -(1/2)\{p_2 C_3^2 (1 + \eta^2/3) + p_1 \nu_o^2\}. \tag{33}$$

The coefficient of F^{n-3} is given by the negative of the sum of the 3 x 3 minors along the diagonal of the secular determinant. Brown's result for this calculation is,

$$a_3 = -1/3\{p_3 C_3^3 (1 - \eta^2) + 3p_2 \nu_o^2 C_3 (3\cos^2\theta - 1 + \eta \sin^2\theta \cos 2\phi)\}. \tag{34}$$

Insertion of Eq. [34] into Eq. [26] yields the resulting moment expressions,

$$S_1 = 0,$$
$$S_2 = p_2 C_3^2 (1+\eta^2/3) + p_1 \nu_o^2, \tag{35}$$
$$S_3 = p_3 C_3^3 (1-\eta^2) + 3 p_2 \nu_o^2 C_3 (3\cos^2\theta - 1 + \eta \sin^2\theta \cos 2\phi),$$

where p_1, p_2, and p_3 are defined as,

$$p_1 = 2I(I+1)(2I+1)/3!,$$
$$p_2 = 2I(I+1)(2I-I)(2I+3)/3(5!), \tag{36}$$
$$p_3 = 2I(I+1)(2I-3)(2I-1)(2I+1)(2I+3)(2I+5)/3(7!),$$

ν_o is the Larmor frequency, C_3 is the frequency interval between pure quadrupole transition frequencies with $\eta = 0$, I is the nuclear spin, and the angles θ and ϕ are the polar and azimuthal angles, respectively, of the vector H_o in the xyz system (see Figure 3).

Whitehouse, Ray, and Royer (41) extended the results of Brown (37) and Parker (40) such that Eq. [35] could be used in the absence of a knowledge of the angles θ and ϕ. By a consideration of Figure 3 and by application of spherical trigonometry, the angles θ and ϕ may be expressed in terms of the angles α, β, and δ.

The mutually perpendicular axes a, b, and c form the laboratory coordinate system which can be related in some known manner to either crystal axes or faces. Vector OC gives the direction of the z-principal axis of the electric field gradient (the ϕ_{zz} direction). The x- and y-axes define the directions, ϕ_{xx} and ϕ_{yy}, of the electric field gradient. α is the angle between the b-axis and the projection of the ϕ_{zz} direction

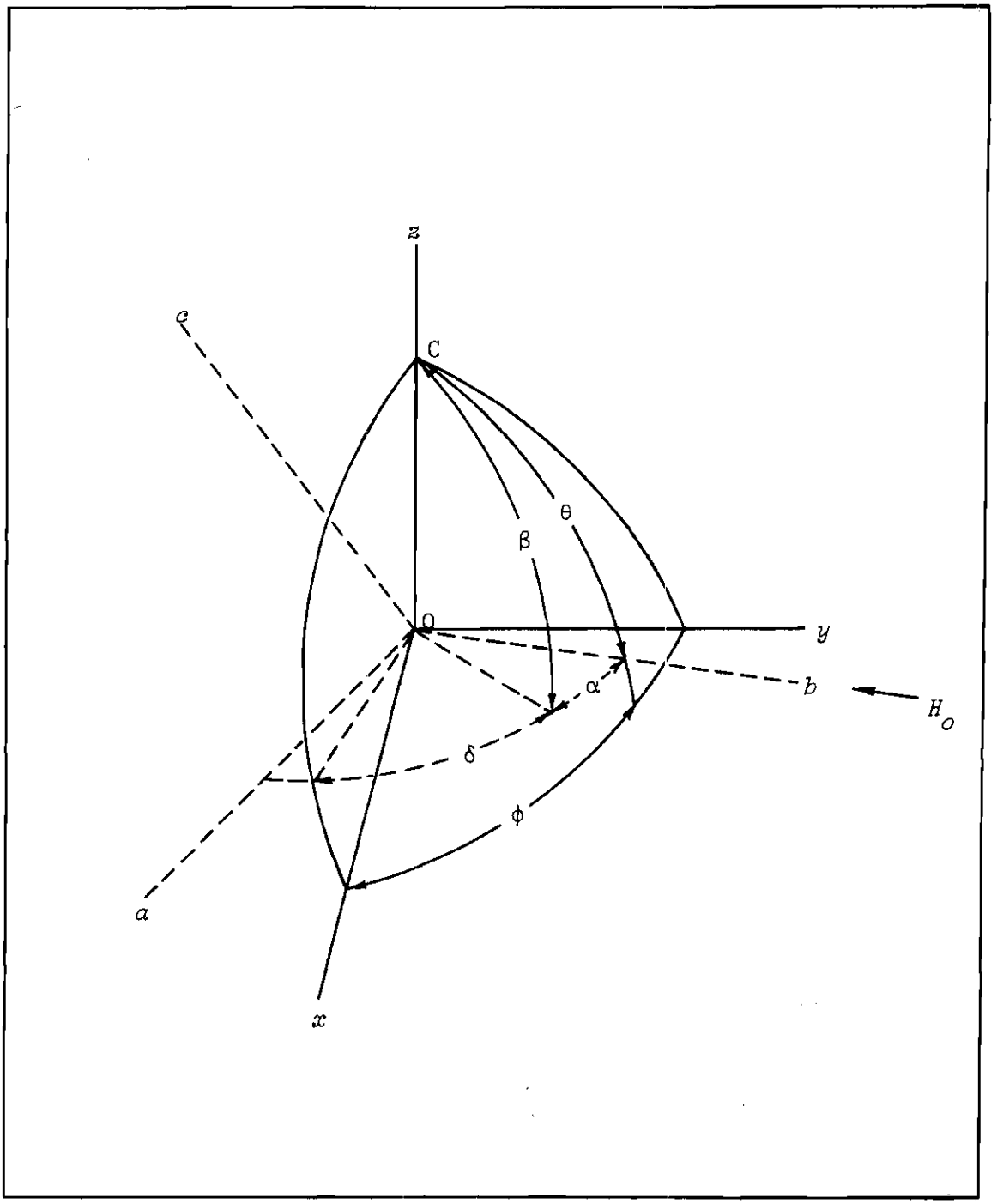

Figure 3. Generalized Coordinate Axis System

on the *ab* plane. β is the angle between the ϕ_{zz} direction and its projection on the *ab* plane. δ is the angle between the ϕ_{zz} projection on the *ab* plane and the *xz* plane.

By straightforward mathematical manipulation the expression,

$$S_3 = A_1 + A_2 cos2\alpha + A_3 sin2\alpha, \tag{37}$$

where

$$\begin{aligned} A_1 &= F+G\eta[2sin^2\delta/(1-cos^2\beta cos^2\delta)-1]+A_2, \\ A_2 &= 3/2G cos^2\beta+1/2G\eta(2cos^2\delta sin^2\beta-cos^4\beta cos^2\delta+cos^2\beta-2sin^2\delta)/ \\ &\qquad (1-cos^2\beta cos^2\delta), \\ A_3 &= -2G\eta sin^2\beta sin\delta cos\delta/(1-cos^2\beta cos^2\delta), \\ F &= p_3C_3^3(1-\eta^2)-3p_2\nu_o^2C_3, \\ G &= 3p_2\nu_o^2C_3, \end{aligned} \tag{38}$$

results. By reorienting the principal axis system, i.e., by rotating the crystal through an angle *r*, α becomes α+*r* (β, δ, A_1, A_2, and A_3 are unchanged) and Eq. [37] becomes,

$$S_3 = A_1 + A_2 cos2(\alpha+r) + A_3 cos2(\alpha+r). \tag{39}$$

Rotation of the crystal about a second axis yields a second set of values for A_1, A_2, A_3, and α which when combined with the first set locates the *z*-axis of the electric field gradient and fixes the value of β. Substitution of β into the A_n expressions allows the evaluation of C_3 ($C_3 = 3e^2Qq/((2I)(2I-1)h)$).

The resonance frequencies were computer fitted to Eq. [37] by means of a nonlinear least squares procedure (42). Because of the complexity of the A_n expressions, the calculated values for these inter-

mediate parameters were not used to calculate the remaining parameters, C_3, η, and δ, but rather the following procedure was used. The calculated values of α and β for each rotation were substituted into Eq. [37], and the resulting equation was rearranged and simplified as much as possible. The equation was then least squares fitted to the data a second time directly in terms of C_3, η, and δ.

Whitehouse, Ray, and Royer (41) also gave an expression for S_3 for a powdered sample. Their expression was,

$$p_3 C_3^3(1-\eta^2)+3p_2\nu_o^2 C_3(\eta-1)-S_3 = 0 \qquad (40)$$

Thus, values of the quadrupole coupling constant and the asymmetry parameter may be gleaned from observed resonance frequencies in a powdered sample.

CHAPTER III

EXPERIMENTAL

Chemicals

The following chemicals were obtained as reagent grade, unless otherwise specified, and were used without further purification.

Absolute ethanol

Acetone

Aqueous ammonia

Arsenic(V) oxide

Catechol

Cinchonine

Cobalt(II) chloride hexahydrate

Deionized water

Ethylenediamine (98%)

Hydrobromic acid (47-49%)

Nitric acid

Potassium hydroxide

1,2-Propanediamine (90%)

1,3-Propanediamine (practical)

Silver nitrate

Sodium bromide

Sodium chloride

Sodium iodide

Sodium nitrate

d-Tartaric acid

Triethylenetetramine (technical)

Conventional abbreviations are used for the amine ligands. These abbreviations are

Ethylenediamine - en

1,2-Propanediamine - pn

1,3-Propanediamine - tn

Triethylenetetramine - trien.

Preparation and Resolution of Complexes

Because of the large amount of material required by the nmr experiments, most of the preparations and resolutions were carried out several times each. Typical results are described in each case. Percentage yields were not determined, and no attempt was made to maximize the yields, but most of the yields were good.

Sodium *Tris*-(ethylenediamine)cobalt(III) Chloride Hexahydrate

This material was prepared by a method which is a slight modification of the one described by Work (43). Solutions of cobalt(II) chloride hexahydrate (23.8 g; 0.1 mol) in 50 ml of water and hydrochloric acid (8.7 ml of 12M; 0.1 mol) were mixed in a 250 ml beaker. Ethylenediamine (18.4 g; 0.3 mol) was placed in a 250 ml filter flask equipped with an air delivery tube. The acidic solution of cobalt(II) chloride was slowly added with swirling to the ethylenediamine. Bone charcoal (4 g) was added to the reaction vessel and a brisk stream of air was pulled first through an aqueous sodium hydroxide solution then through

the reaction mixture. Aeration was continued for four hours.

The charcoal was removed by filtration and was washed several times with hot water (approximately 200 ml total volume). The filtrate and washings were combined and concentrated with a vacuum rotary evaporator over boiling water to about one-third of the initial volume. After cooling, an equal volume of absolute ethanol was added to the solution and the resulting mixture was cooled in an ice-bath. Orange crystals of $[Co(en)_3]Cl_3 \cdot 3H_2O$ precipitated from the solution. The crystals were collected on a buchner funnel and were washed with acetone and sucked very dry.

Conversion to the mixed salt, $\{[Co(en)_3]Cl_3\}_2 \cdot NaCl \cdot 6H_2O$, was effected by preparing an aqueous solution containing a five to three ratio by weight of $[Co(en)_3]Cl_3 \cdot 3H_2O$ to NaCl (19). By slowly evaporating this solution, crystals of the desired salt were obtained. Confirmation of composition was made by checking the water content. Water was determined by dehydration of the material in an oven at 110°C. The percentage of water in a sample of the material was 12.0 per cent as compared to the calculated percentage of 12.6 per cent.

Sodium $\Lambda(+)_{589}$-*Tris*-(ethylenediamine)cobalt(III) Chloride Hexahydrate

The procedure used for the preparation of this compound was a very slight modification of the partial asymmetric synthesis for preparing $\Lambda(+)_{589}[Co(en)_3]I_3 \cdot H_2O$ as outlined by Broomhead, Dwyer, and Hogarth (44). Cobalt(II) *d*-tartrate was prepared by combining equimolar mixtures of cobalt(II) sulfate heptahydrate and sodium *d*-tartrate each in aqueous solution. Ethylenediamine (20.4 ml of 88.6%; 0.3 mol) was placed in a 500 ml filter flask fitted with a rubber stopper and a wide

glass tube for entry of air. After dilution with water (50 ml) and ethanol (30 ml), the mixture was cooled in ice. Hydrochloric acid (10 ml of 10M; 0.1 ml) was added slowly with stirring, and the solution was cooled to 4 to 8°C in an ice bath. The cobalt(II) *d*-tartrate (20.7 g; 0.1 mol) was added slowly with stirring. Animal charcoal (4 g) was added and a stream of air pulled through for 2 hours.

The product, which was mixed with charcoal, was filtered off and washed with 40 per cent ethanol (60 ml) and the washings were discarded. The diastereoisomer, $\Lambda(+)_{589}[Co(en)_3]Cl(d\text{-tart})$, was extracted with successive portions of hot water (60°C). The extract was concentrated by evaporation to a volume of 50 ml, and on cooling in ice, the pure diastereoisomer precipitated. Conversion to $\Lambda[Co(en)_3]I_3 \cdot H_2O$ was effected by stirring with 35 g of sodium iodide dissolved in 50 ml of water.

The only differences to the foregoing procedure and this work were that cobalt(II) chloride hexahydrate was substituted for cobalt(II) sulfate heptahydrate, 98 per cent ethylenediamine was used instead of 88.6 per cent, and the iodide salt was converted to the chloride salt. Conversion of $\Lambda[Co(en)_3]I_3 \cdot H_2O$ to $\Lambda[Co(en)_3]Cl_3 \cdot 3H_2O$ was accomplished by stirring an aqueous solution of the iodide salt with an excess of silver chloride. The excess silver chloride and the silver iodide were removed by filtration. The chloride salt was then precipitated from the solution by addition of an equal volume of ethanol followed by cooling in an ice bath. The chloride salt thus obtained was converted to the mixed salt $\{\Lambda[Co(en)_3]Cl_3\}_2 \cdot NaCl \cdot 6H_2O$, as in the previous synthesis. The specific rotation of the iodide salt at 589 mμ was determined to be +90° which is identical to the reference value (44).

Tris-(1,3-propanediamine)cobalt(III) Chloride (45)

A solution of cobalt(II) chloride hexahydrate (48 g; 0.2 mol) in approximately 200 ml of water was added to 1,3-propanediamine (45 g; 0.61 mol) contained in a filter flask equipped with a glass air delivery tube. Hydrochloric acid (17 ml of 12M; 0.2 mol) was slowly added to the resulting solution. Ten grams of bone charcoal was added to the partially neutralized solution. The cobalt was oxidized by pulling a brisk stream of air first through an aqueous sodium hydroxide solution and then through the reaction mixture. Aeration time was approximately eight hours.

The charcoal was removed by filtration and washed with water. The filtrate and washings were combined and the solution was concentrated with a vacuum rotary evaporator over boiling water to about one-third of the initial volume, then 30 ml of 12M hydrochloric acid was added. After cooling, an equal volume of absolute ethanol was added to induce precipitation. The pink salt that formed was collected on filter paper and was recrystallized from water by addition of absolute ethanol, collected on filter paper, and washed with acetone. This salt appeared to be anhydrous, since no weight loss was observed on heating at 110°C for several days. Conversion to the bromide or nitrate salts was accomplished by addition of hydrobromic acid or nitric acid, respectively, to aqueous solutions of the chloride salt. The nitrate salt appeared to be anhydrous, since no weight loss on heating to 110°C was observed. The bromide salt had a water content corresponding to the monohydrate, $[Co(tn)_3]Br_3 \cdot H_2O$ (3.41 per cent compared to 3.34 per cent theoretical). In each case, evaporation of the solution followed by cooling in an ice bath resulted in formation of the desired salt.

$\Delta(+)_{589}$-*Tris*-(1,3-propanediamine)cobalt(III) Chloride

The racemic salt, $[Co(tn)_3]Cl_3$, was prepared in the previous synthesis. An aqueous solution of this salt was prepared and to this solution was added an aqueous solution of the potassium salt of the *levo* complex anion of arsenic(V) with catechol (potassium *l*-*tris*-catecholatoarsenate(V)). This salt was prepared by the method of Ryschkewitsch and Garrett (46). The molar ratio of the cobalt salt to the complex anion was one to one and one-half. A precipitate formed which was collected on a sintered glass filter. The solid was treated with concentrated (12M) hydrochloric acid (25 ml) and this treatment yielded a solution of $\Delta(+)_{589}[Co(tn)_3]^{+++}$ and the racemized arsenic(V) catechol complex. The solution was filtered through the sintered glass filter.

On concentration by evaporation under vacuum over a boiling water bath followed by cooling and addition of acetone the salt $\Delta(+)_{589}[Co(tn)_3]Cl_3$, precipitated. The racemized salt of the arsenic(V) catechol complex remained in solution.

Purification of the optically active cobalt salt was accomplished by repeated recrystallization of the salt until a constant specific rotation was obtained. Five recrystallizations were found to be sufficient. The only other reported resolution of this complex ion was performed by Woldbye (47) using nitro *d*-camphor. The molecular rotation at 589 mμ was 360° as compared to ≈360° as reported by Woldbye (48). Woldbye (48) has also measured the solution ORD and CD of this ion.

The bromide and nitrate salts of this ion were prepared as in the previous synthesis.

d-1,2-Propanediamine

Racemic 1,2-propanediamine was resolved according to the method described by Dwyer, Garvan, and Shulman (49). Racemic 1,2-propanediamine (260 g; 3.51 mol) was slowly added with stirring to a solution of *d*-tartaric acid (700 g; 4.67 mol) in cold water (750 ml). The mixture was cooled slowly to about 25°C and was then rapidly cooled in an ice bath to about 4°C. The crystalline diastereoisomer that formed was removed by filtration on a buchner funnel and was washed with ice water. The filtrate and washings were combined and glacial acetic acid was added. On standing overnight, more crystals were obtained. These crystals were removed by filtration as before.

The filtrate was evaporated in an evaporating dish on a boiling water bath. A thick syrup was left which was placed in a two-liter three-necked flask. Sodium hydroxide pellets were added in large excess. The mixture was distilled by heating and pulling a stream of air through the mixture for agitation. The distillate contained approximately 130 g of the *dextro* isomer of the 1,2-propanediamine. The specific rotation at 589 mμ was +34°.

$\Lambda(+)_{589}$-*Tris*-(*d*-1,2-propanediamine)cobalt(III) Bromide

The distilled *d*-1,2-propanediamine (130 g) was partially neutralized with 12M hydrochloric acid (18.5 ml of 12M) and transferred to a one-liter flask. Cobalt(II) *d*-tartrate (46 g) was added slowly with stirring to the amine solution. Charcoal (12 g) was added to this mixture and a brisk current of air was pulled first through an aqueous sodium hydroxide solution and then through the reaction mixture. Aeration time was for twenty-four hours. The charcoal was filtered from the solu-

tion and washed with hot water (100 ml). The filtrate and washings were combined and evaporated to approximately 200 ml on a boiling water bath. The solution was cooled to room temperature and absolute ethanol (250 ml) was added. A red oil formed on cooling in an ice bath and this oil was isolated by decanting the less viscous material from the oil. Crystallization was effected by adding absolute ethanol to the oil. A good yield of pure $\Lambda(+)_{589}[Co\{(+)\text{-}(pn)_3\}\delta\delta\delta]Cl(d\text{-tart})\cdot 3H_2O$ was obtained. Conversion to the iodide salt was effected by treating a solution of the mixed chloride *d*-tartrate (5 g in 20 ml of water) with aqueous ammonia (0.2 ml of 15M) and adding an aqueous solution of sodium iodide. Upon cooling, crystals of $\Lambda[Co(d\text{-pn})]_3I_3\cdot 3H_2O$ precipitated from the solution. The specific rotation at 546 mμ was +184° and was identical to the reference value (49).

Conversion to the chloride or bromide salts was accomplished by stirring with silver chloride or silver bromide, respectively. The bromide salt was analyzed for water content and was found to be anhydrous.

A smaller quantity of the salt $\Lambda[Co(d\text{-pn})_3]Br_3$ was prepared by a second method. Iwasaki and Saito (22) reported the preparation of $\Delta[Co(l\text{-pn})_3]Br_3$. The enantiomorph of this compound was prepared in a similar fashion. Distilled *d*-1,2-propanediamine (5.5 g), prepared as above, was heated with 5.0 g of chloropurpureo-salt, $[Co(NH_3)_5Cl]Cl_2$, until evolution of ammonia ceased. The reaction mixture was dissolved in a minimum amount of water and hydrobromic acid was added in excess. On cooling the resulting solution in an ice bath, crystals of $\Lambda[Co(d\text{-pn})_3]Br_3$ were precipitated.

Tris-(triethylenetetramine)dicobalt(III) Nitrate Hexahydrate

Basolo (25) reported the preparation of $[Co_2(trien)_3]Cl_6$ and $[Co_2(trien)_3]I_6$. A solution of triethylenetetramine (75 g; 0.5 mol) in 525 ml of water was added, with stirring, to a solution of cobalt(II) chloride hexahydrate (160 g; 0.67 mol) in 500 ml of water. The mixture was placed in a two-liter filter flask equipped with a glass delivery tube for entry of air, and a vigorous stream of air was pulled first through an aqueous sodium hydroxide solution and then through the reaction mixture. Aeration was continued for about twelve hours. Concentrated hydrochloric acid (350 ml of 12M) was added, and the solution was concentrated by a rotary vacuum evaporator over boiling water to a volume of about 400 ml and cooled whereupon a bluish-purple crystalline product formed. The precipitate was collected on a buchner funnel and washed successively with cold water, absolute ethanol, and ether. The salt, *cis*-dichlorotriethylenetetraminecobalt(III) chloride, was dried in an oven at 110°C.

Twenty grams (0.064 mol) of the material prepared as above and 9.6 g (0.065 mol) of triethylenetetramine, and 300 ml of absolute ethanol were placed in a two-liter three-necked flask equipped with a mechanical stirrer and reflux condenser. The mixture was allowed to reflux with vigorous stirring for eight hours. The mixture was then filtered hot, and the orange precipitate ($[Co_2(trien)_3]Cl_6$) that was collected was washed with absolute ethanol and then ether. Unless this prescribed filtering and washing procedure was followed, a considerable amount of excess amine remained in the precipitate.

Conversion to the nitrate salt was accomplished by addition of an aqueous solution of sodium nitrate to an aqueous solution of $[Co_2(trien)_3]Cl_6$. Good yields of $[Co_2(trien)_3](NO_3)_6 \cdot 6H_2O$ were obtained by this method. Confirmation of composition was made by checking the water content. A sample of the nitrate salt contained 10.11 per cent water, compared to the calculated amount of 10.43 per cent for the hexahydrate. This salt was not stable when left in air, as it appeared to dehydrate.

$(+)_{589}$-*Tris*(triethylenetetramine)dicobalt(III) Chloride

The racemic salt of this compound was prepared in the previous synthesis. An aqueous solution of this salt was prepared and to this solution was added an aqueous solution of potassium *l-tris*-catecholatoarsenate(V). In the first attempt at resolution by this method, the molar ratio of the cobalt salt to the complex anion was one to three. However, this much anion precipitated all the cobalt from the solution. In the subsequent precipitations, the complex anion solution was added dropwise with care being taken to prevent precipitation of all of the cobalt. The precipitate that formed was collected on a sintered glass filter, washed with water, and finally treated with 25 ml of concentrated hydrochloric acid (12M). This treatment yielded $(+)_{589}$-$[Co_2(trien)_3]^{6+}$ and the racemic arsenic(V)-catechol complex in solution. The solution was filtered through the sintered glass filter. On concentration by evaporation under vacuum on a boiling water bath followed by addition of acetone, the salt, $(+)_{589}[Co_2(trien)_3]Cl_6$, precipitated. The racemized salt of the arsenic(V)-catechol complex anion remained in solution. Purification of the optically active material was accomplished by recyrs-

tallizing four or five times from aqueous solution. No previous reports for the resolution of this salt have been found. The molecular rotation of $(+)_{589}[Co_2(trien)_3]Cl_6$ at 546 mμ was +443°.

Optical Experiments

All the optical experiments were performed at 25 ± 1°C.

Solution Spectra

The absorption spectra presented herein were obtained by either a Beckman DK-1 Recording Spectrophotometer or a Japan Spectroscopic Co., Ltd. ORD/UV-5 Spectrometer. Agreement between the two instruments was excellent. Matched quartz cuvettes were consistently used in these experiments.

The ORD and CD data presented herein were obtained by use of a Japan Spectroscopic Co., Ltd. ORD/UV-5 Spectrometer. A strain-free quartz cuvette was used for the solution ORD and CD measurements. A standard camphor sulfonic acid solution was used to calibrate the instrument.

Routine checks of optical rotation were made with a Bendix-Ericsson Automatic Polarimeter, Type 143A. The cell used for these measurements was an all Pyrex glass cell equipped with a jacket to allow control of temperature in the cell. The path length of the cell was 4.87 cm and the volume of the cell was 7.35 ml.

Single Crystal Spectra

Single crystal electronic absorption and CD spectra were obtained for compounds containing each of the optically active cobalt complex ions previously mentioned with the exception of $(+)_{589}[Co_2(trien)_3]^{6+}$.

Apparently, no structure of a compound containing this ion has been determined. Thus, no single crystal spectra were measured since the orientation of the ion with respect to the crystallographic axes was needed in order to obtain meaningful data.

The compounds that gave suitable crystals for this study were $\{\Lambda[Co(en)_3]Cl_3\}_2 \cdot NaCl \cdot 6H_2O$, $\Delta[Co(tn)_3]Cl_3 \cdot 4H_2O$, and $\Lambda[Co(d\text{-pn})_3]Br_3$. The habits of these crystals are shown in Figure 4.

Crystals of $\{\Lambda[Co(en)_3]Cl_3\}_2 \cdot NaCl \cdot 6H_2O$ were readily obtained by slow evaporation from an open beaker of an aqueous solution of this salt. The crystals thus obtained were very well formed and of a suitable thickness and cross-sectional area for the optical experiments. The crystals that were selected were hexagonal plates, the faces of which were perpendicular to the c-axis of the crystal.

Crystals of $\Lambda[Co(d\text{-pn})_3]Br_3$ were extremely difficult to obtain. Slow evaporation of the aqueous solution of the salt from an open beaker resulted in formation of very finely divided crystals of too small a size for use in the optical experiments. The best method found was to slowly evaporate an aqueous solution of the salt from an open tube. The actual tube size was 14 mm outside diameter by 30 cm long. The tube was filled with an aqueous solution of the salt and then placed in a constant temperature box at 35°C. After about three weeks, usable crystals had formed on the walls of the tube. These crystals had the same habit as the crystals of $\{\Lambda[Co(en)_3]Cl_3\}_2 \cdot NaCl \cdot 6H_2O$, namely hexagonal prismatic.

Crystals of $\Delta[Co(tn)_3]Cl_3 \cdot 4H_2O$ were obtained by crystallization of the salt from an ethanol-water mixture. The water content was determined by dehydration at 110°C, and the experimentally determined water

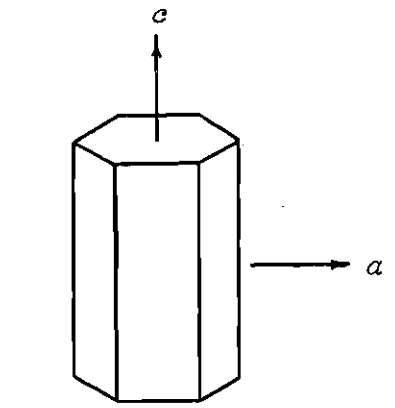

$\{\Lambda[Co(en)_3]Cl_3\}_2 \cdot NaCl \cdot 6H_2O$

$\Lambda[Co(d\text{-}pn)_3]Br_3$

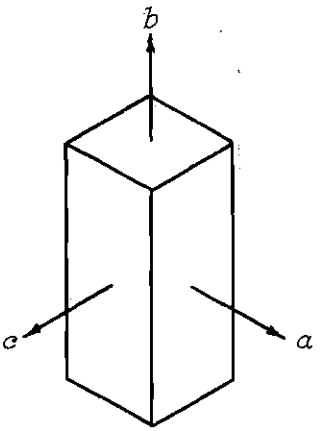

$\Delta[Co(tn)_3]Cl_3 \cdot 4H_2O$

Figure 4. Habits of Crystals Used in Single Crystal Circular Dichroism Experiments

content (16.6 per cent) corresponds to the tetrahydrate (15.7 per cent). This salt was especially unstable with respect to dehydration and appeared to dehydrate when exposed to the atmosphere. Thus, the crystals used in the experiments were always quickly coated with mineral oil after removal from the precipitating medium. The habit of the crystal thus obtained is shown in Figure 4. The crystals obtained for use in the optical experiments were rhombic plates, the faces of the plates being perpendicular to the *b*-axis of the crystal.

The mount for the crystals consisted of a cylinder of aluminum (0.865 in diameter by 1 in long) with a concentric hole bored parallel to the cylindrical axis. This mount was used because it could be fitted snugly into the instrument used for the CD measurements. Also, the mount permitted duplicate experiments to be performed with assurance of identical positioning of the crystal. A glass disk was affixed to the aluminum cylinder. A crystal of each compound to be studied was placed in turn on the glass disk and secured by means of Scotch No. 33 Vinyl Plastic Electrical Type. In each case, the crystal was mounted such that the prismatic face was perpendicular to the direction of propagation of light. Care was taken to ensure that all of the light passed through the sample. Each crystal was then coated with mineral oil to prevent dehydration.

In obtaining the visible absorption spectra, an identical cell was placed in the reference beam. Base lines using the above mentioned cells were always determined. No significant change in base line was ever observed over the wavelength range studied.

Single crystal CD experiments were performed using the same type

cell as that used for obtaining the single crystal absorption spectra. Camphor sulfonic acid was used for calibration of the spectrometer used for the CD measurements.

Nuclear Magnetic Resonance Experiments

Preparation of Single Crystals for NMR Studies

Single crystals of $[Co(tn)_3]Cl_3 \cdot 4H_2O$, $[Co(tn)_3](NO_3)_3$, $\{[Co(en)_3]Cl_3\}_2 \cdot NaCl \cdot 6H_2O$, and $[Co_2(trien)_3](NO_3)_6 \cdot 6H_2O$ were prepared by the diffusion method (42). The materials for growing the crystals were prepared as previously described in this chapter.

In all instances except one, seed crystals were obtained by preparing supersaturated solutions of the desired material and allowing the crystals to precipitate from these solutions. In each instance, the solution was contained in an Erlenmeyer flask capped with polyethylene film. The exception to this procedure was the preparation of seed crystals of $[Co(tn)_3]Cl_3 \cdot 4H_2O$. Aqueous solutions of $[Co(tn)_3]Cl_3$ were prepared, and absolute ethanol was added until a medium to heavy precipitate of $[Co(tn)_3]Cl_3$ formed. The solutions were contained in Erlenmeyer flasks and the flasks were capped with polethylene film. Solution of the $[Co(tn)_3]Cl_3$ in the ethanol-water mixture was effected by heating. On standing and cooling to room temperature, well formed crystals of $[Co(tn)_3]Cl_3 \cdot 4H_2O$ formed.

In a typical single crystal growth, the seed crystal was mounted on a glass stopper at a desired orientation. The stopper was inserted into a 50 cm long, 14 mm o.d. tube and was glued in place. The tube was filled with a saturated (at 29°C) solution of the seed crystal material (the solution from which the seed was obtained). The tube was

then placed in a two-compartment constant temperature box. The top compartment was maintained at 35°C and the bottom compartment was maintained at 29°C. A glass-wool plug was inserted into the tube and pushed to the junction between the two compartments.

A few milligrams of solid material was added to the solution in the tube each day. The solid material, which rested on the glass-wool plug, dissolved in the high-temperature region, diffused to the cooler region, and crystal growth of the seed crystal occurred. Crystal growth was continued until a crystal about four centimeters long that filled the tube was grown. Growth periods ranged from about three weeks to about two months. The solution was drained from the tube and the tube was then cut to a length of 30 cm and a three-inch protractor was affixed to the top of the tube.

Nuclear Magnetic Resonance Spectra

A Varian DP-60 Dual Purpose Nuclear Magnetic Resonance Spectrometer, equipped with a 15.085 MHz fixed frequency oscillator-receiver unit, was used to obtain the ^{59}Co nmr data presented here. A block diagram showing the major equipmental components of this system is shown in Figure 5.

In a typical experiment, the tube containing the single crystal was placed in the nmr probe, and the magnetic field was varied over the desired range. The actual measurements that were made were magnet current values at the resonance positions. Conversion of these measured current values to magnetic field values was accomplished by means of a magnetic field versus magnet current calibration curve. This curve was constructed by using aqueous solutions of salts containing nuclei of

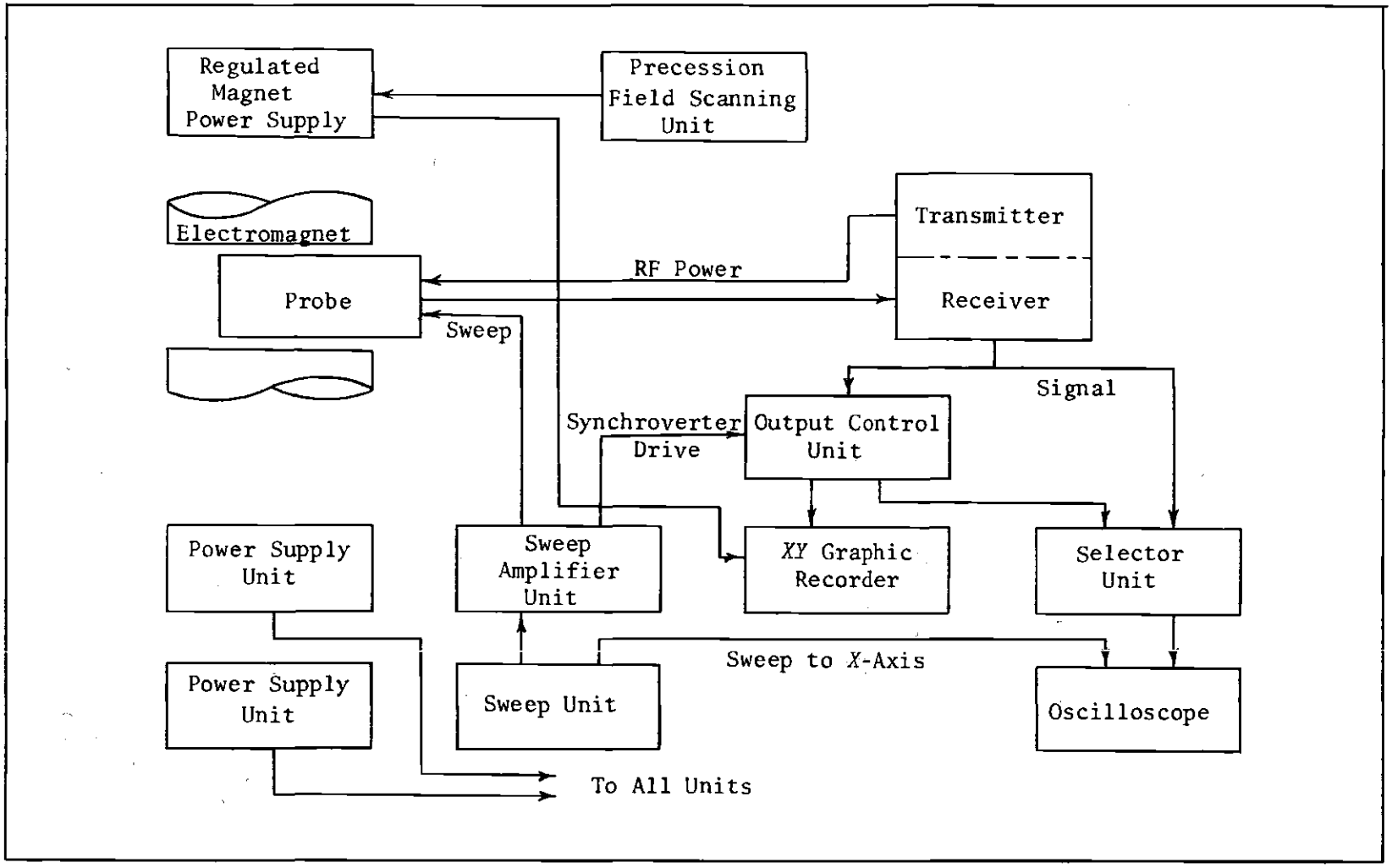

Figure 5. Block Diagram of
Nuclear Magnetic Resonance Spectrometer

known resonance frequencies. This calibration curve is shown in Figure 6. The resonant nuclei are indicated by mass-number superscripts, e.g., $[^{59}Co(en)_3]Cl_3$ indicates that the resonance position of ^{59}Co was determined in an aqueous solution of the indicated salt.

The crystal was rotated coaxially with the divided circle of the protractor about an axis perpendicular to the polarizing magnetic field, H_o. A rotation of 180° corresponded to a rotation of H_o about the origin in the xyz system so that H_o remained perpendicular to the growth axis of the crystal which was along the axis of the tube. The reference position of the crystal was established by means of the protractor attached to the top of the tube. An index for the protractor was provided by means of an etched piece of "plexiglass" that was placed between the pole faces of the magnet. The protractor, and thus the crystal position, was measurable to ±0.25°. Spectral patterns were obtained at 10° intervals.

Since a single crystal of $\Lambda[Co(d\text{-pn})_3]Br_3$ of a suitable size for the nmr studies could not be grown, a powdered sample of this material was used. The powder was placed in a 14 mm outside diameter test tube. The nmr spectrum for this material was obtained in the same fashion as for the single crystals. The resulting spectrum was of much poorer quality than the single crystal spectra.

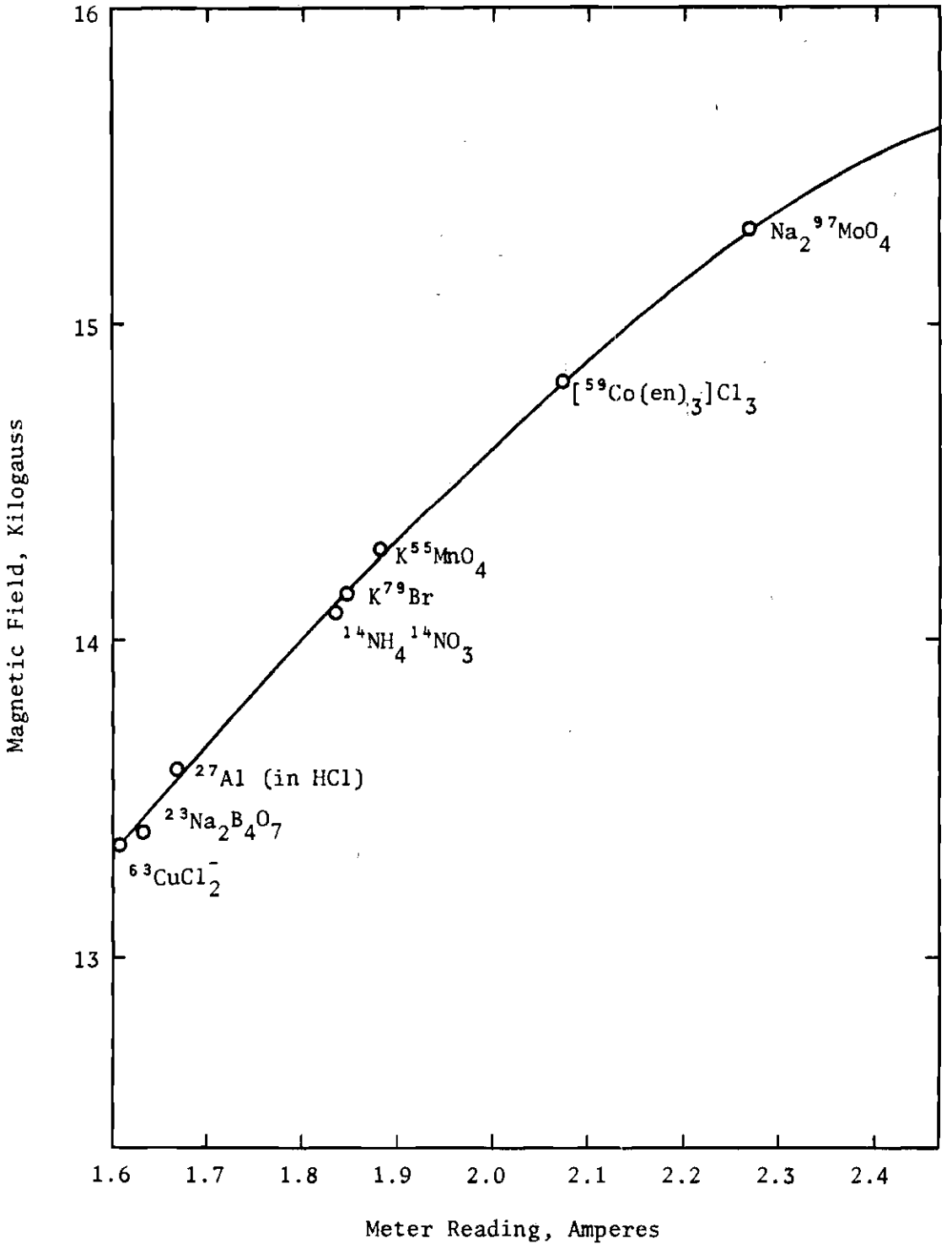

Figure 6. Magnet Calibration Curve

CHAPTER IV

RESULTS

Optical Experiments

Sodium $\Lambda(+)_{589}$-*Tris*-(ethylenediamine)cobalt(III) Chloride Hexahydrate

The C_3 axis of the complex ion, $\Lambda[Co(en)_3]^{+++}$, in the hexagonal double salt, $\{\Lambda[Co(en)_3]Cl_3\}_2 \cdot NaCl \cdot 6H_2O$, was found by X-ray diffraction (19) to be parallel to the prismatic axis of the crystal, i.e., the *c*-axis as shown in Figure 4. McCaffery and Mason (17) measured the CD, ORD, and electronic absorption spectra of this ion both in aqueous solution and in the previously mentioned double salt. Drouard and Mathieu (50) made similar measurements on the compound, $\Lambda[Co(en)_3]Br_3 \cdot H_2O$ (20). The measurements made by the two groups of workers were in reasonable agreement, and the results of the electronic absorption and CD measurements are summarized in Table 1.

The values of the dipole strengths, D, and rotational strengths, R, were recalculated on the basis of Gaussian shape functions for the absorption and CD curves, respectively. The mathematical expression for the calculation of rotational strength on the basis of a Gaussian shape function was given previously (Eq. [9]). For the calculation of dipole strength on this basis, Eq. [10] yields,

$$D \simeq 98 \times 10^{-40} \cdot \varepsilon_{max} \cdot \Delta\nu_{1/2}/\nu_o, \qquad (41)$$

where ε_{max} is the maximum value of the molar decadic extinction coeffici-

Table 1. Absorption and Circular Dichroism Data for Compounds Containing $\Lambda[Co(en)_3]^{3+}$

System	Absorption				Circular Dichroism			
	ν_o(kK)	$\Delta\nu_{1/2}$(kK)	ε_{max}	$D(10^{-40}$cgs)	ν_o(kK)	$\Delta\nu_{1/2}$(kK)	$(\varepsilon_l-\varepsilon_r)_{max}$	$R(10^{-40}$cgs)
$[Co(en)_3]^{3+}$* (Aqueous Solution)	21.322	3.40	84	1313	20.284 23.364	2.00 1.50	1.89 -0.17	4.57 -0.26
$\Lambda[Co(en)_3]Br_3\cdot H_2O$** (Single Crystal)	21.277	3.60	117	1940	20.833	3.40	+18	72
$\{\Lambda[Co(en)_3]Cl_3\}_2\cdot NaCl\cdot 6H_2O$* (Single Crystal)	21.413	3.70	95	1608	21.053	3.10	+23.3	84

*Reference 17

**Reference 50

ent, $\Delta\nu_{1/2}$ refers to the half-width of the absorption band, and ν_o refers to the frequency of maximum absorption.

The ORD, CD, and electronic absorption spectra of aqueous solutions of the double salt, $\{\Lambda[Co(en)_3]Cl_3\}_2 \cdot NaCl \cdot 6H_2O$, were measured. In addition, the CD and electronic absorption spectra of this salt in a single crystal were measured. Agreement with previously reported measurements (17,50) was quite good. The results of the solution and single crystal measurements are given in Tables 2 and 3, respectively. Figure 7 shows the ORD and CD curves for an aqueous solution of the double salt, and Figure 8 shows the solution CD and single crystal CD curves for this salt. Light propagation in the single crystal measurements was parallel to the crystallographic c-axis. For this orientation, the single crystal CD curve should show the $^1A_1 \rightarrow {}^1E_a$ transition only.

A relatively small shift of the position of the maximum in the CD curve was observed in going from the solution to the single crystal. This small shift indicated an appreciable energy splitting of the component bands of the solution CD spectrum.

In order to obtain an approximation of the amount of separation of the component bands, the solution CD spectrum was resolved into two Gaussian peaks. This resolution was accomplished by means of a computer program written by Schievelbein and Swart (51). Input experimental data were the molar decadic differential absorptions at various wavelengths. First estimates for peak positions, heights, and widths were also used as input data. This pattern search program varied the parameters to obtain the best fit of the calculated to experimental values of the differential absorptions. The position of the peak corresponding to the

Table 2. Absorption and Circular Dichroism Data for Aqueous Solutions of the Amine Complexes of Cobalt(III).

Complex	Absorption				Circular Dichroism			
	ν_o(kK)	$\Delta\nu_{1/2}$(kK)	ε_{max}	$D(10^{-40}$cgs)	ν_o(kK)	$\Delta\nu_{1/2}$(kK)	$(\varepsilon_l-\varepsilon_r)_{max}$	$R(10^{-40}$cgs)
$\Lambda[Co(en)_3]^{3+}$	21.439	3.50	86.0	1375	20.513	2.13	+1.91	+4.86
					23.364	1.66	-0.22	-0.38
$\Lambda[Co(d\text{-pn})_3]^{3+}$	21.413	3.87	96.5	1709	20.367	2.10	+1.88	+4.74
					22.936	1.93	-0.49	-1.01
$\Delta[Co(tn)_3]^{3+}$	20.534	3.04	72.3	1050	18.868	1.30	-0.062	-0.11
					21.053	2.37	+0.124	+0.34
$(+)_{589}[Co(trien)_3]^{6+}$	21.459	3.24	100.9	1494	20.161	1.85	+0.313	+0.70
					22.624	1.66	-0.123	-0.22

Table 3. Absorption and Circular Dichroism Data for Single Crystals of the Amine Complexes of Cobalt(III).

Complex	Absorption				Circular Dichroism			
	ν_o(kK)	$\Delta\nu_{1/2}$(kK)	ε_{max}	$D(10^{-40}$cgs)	ν_o(kK)	$\Delta\nu_{1/2}$(kK)	$(\varepsilon_l-\varepsilon_r)_{max}$	$R(10^{-40}$cgs)
$\{\Lambda[Co(en)_3]Cl_3\}_2 \cdot NaCl \cdot 6H_2O$	21.459	3.60	95	1562	21.053	3.28	20.2	76.4
$\Delta[Co(tn)_3]Cl_3 \cdot 4H_2O$	20.534	3.40	81	1308	20.682	2.88	4.6	15.7
$\Lambda[Co(d\text{-}pn)_3]Br_3$	21.413	3.68	118	1994	20.833	3.18	16.7	62.3

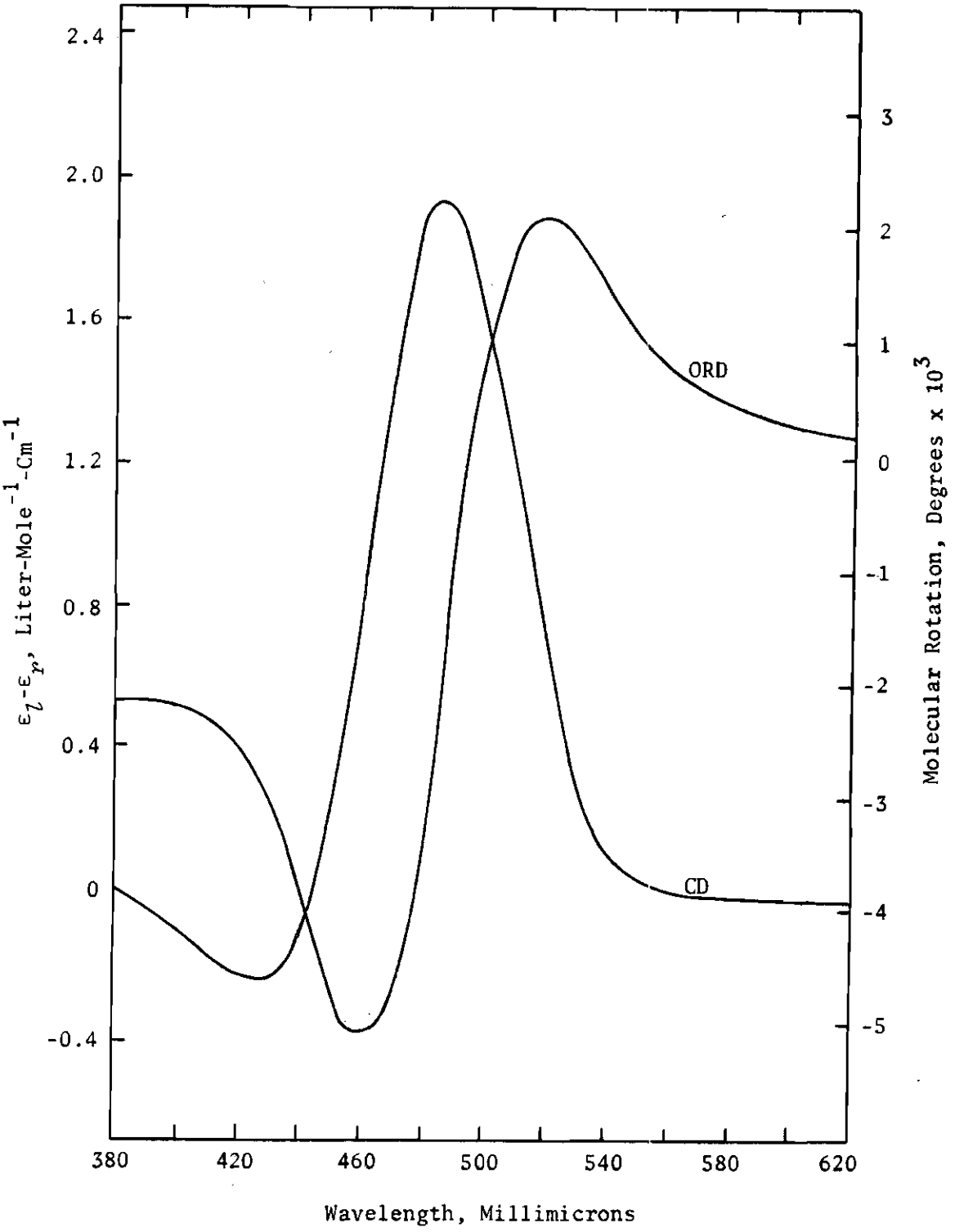

Figure 7. ORD-CD Spectra of $\{\Lambda[Co(en)_3]Cl_3\}_2 \cdot NaCl \cdot 6H_2O$; Aqueous Solution

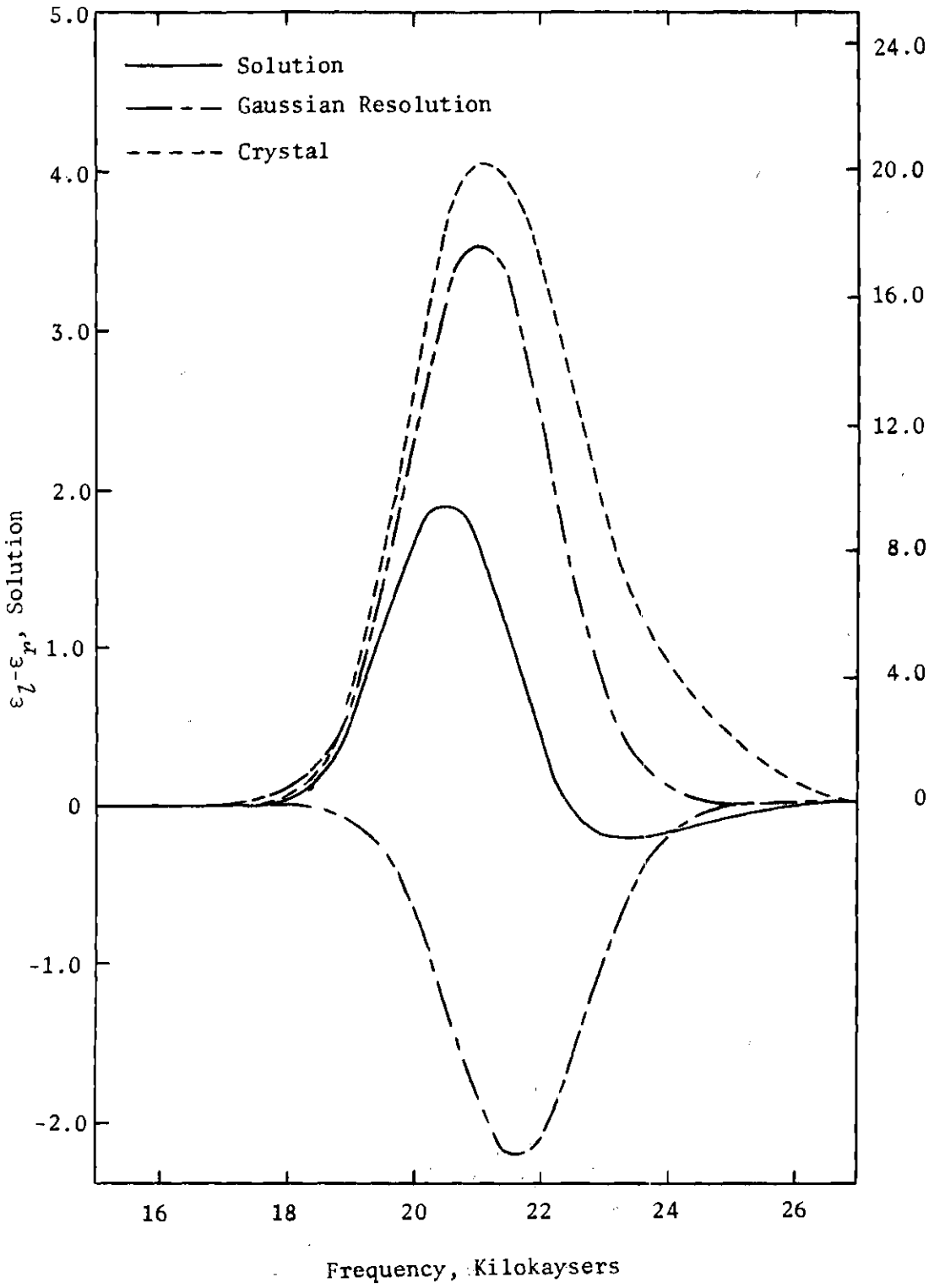

Figure 8. CD Spectra of $\{\Lambda[Co(en)_3]Cl_3\}_2 \cdot NaCl \cdot 6H_2O$

$^1A_1 \rightarrow {}^1E_a$ transition was assumed to be fixed at the position found in the single crystal CD study. The five other parameters were varied and the refinement of each of these parameters was continued until a change in each of these parameters by a factor of 0.002 produced no improvement in the fit. The results of this refinement gave a calculated curve in excellent agreement with the experimental solution curve. In no case were the differences greater than the expected experimental errors in the measured spectra.

The results of the computer resolution are graphically summarized in Figure 8 and the refined parameters are tabulated in Table 4, along with the calculated value of the energy splitting between the two component transitions.

$\Delta(+)_{589}$-*Tris*-(1,3-propanediamine)cobalt(III) Chloride Tetrahydrate

The C_3 axis of the complex ion $\Lambda[Co(tn)_3]^{+++}$ was found by X-ray diffraction (23) to be tilted with respect to the prismatic axis in the rhombic prism crystal of $\Lambda[Co(tn)_3]Br_3 \cdot H_2O$. A similar crystalline habit was observed for the salt, $\Delta[Co(tn)_3]Cl_3 \cdot 4H_2O$, but as will be shown later in this chapter, the three-fold axis of the complex ion, $\Delta[Co(tn)_3]^{+++}$, in this case is parallel to the prismatic axis of the crystal (the *b*-axis as shown in Figure 4) within experimental error.

Electronic absorption, ORD, and CD spectra for an aqueous solution of $\Delta[Co(tn)_3]Cl_3$ were measured. In Figure 9 are shown the ORD and CD spectra for the aqueous solution. The electronic absorption and CD spectra of a single crystal of $\Delta[Co(tn)_3]Cl_3 \cdot 4H_2O$ were measured with light propagation parallel to the crystallographic *b*-axis. With this orientation of the crystal, the CD spectrum should correspond to the

Table 4. Results of the Computer Resolution of Solution Circular Dichroism Spectra Into Component Gaussian Bands

Compound	Band	$(\varepsilon_l-\varepsilon_r)_{max}$	ν_o(kK)	$\Delta\nu_{1/2}$(kK)	$R(10^{-40}$ cgs)	$\nu_E-\nu_A$(kK)
$\{\Lambda[Co(en)_3]Cl_3\}_2\cdot NaCl\cdot 6H_2O$	$^1A_1\rightarrow{}^1E_a$	+3.53	21.053	2.60	+10.7	=0.586
	$^1A_1\rightarrow{}^1A_2$	-2.20	21.639	2.50	-6.2	
$\Lambda[Co(d\text{-pn})_3]Br_3$	$^1A_1\rightarrow{}^1E_a$	+3.08	20.833	2.60	+9.4	-0.863
	$^1A_1\rightarrow{}^1A_2$	-1.68	21.696	3.03	-5.7	
$\Delta[Co(tn)_3]Cl_3\cdot 4H_2O$	$^1A_1\rightarrow{}^1E_a$	+0.207	20.683	3.40	+0.83	+1.506
	$^1A_1\rightarrow{}^1A_2$	-0.136	19.176	2.22	-0.39	
$(+)_{589}[Co_2(trien)_3]Cl_6$		+0.361	20.259	2.13	+0.93	±1.863
		=0.144	22.122	2.75	-0.44	

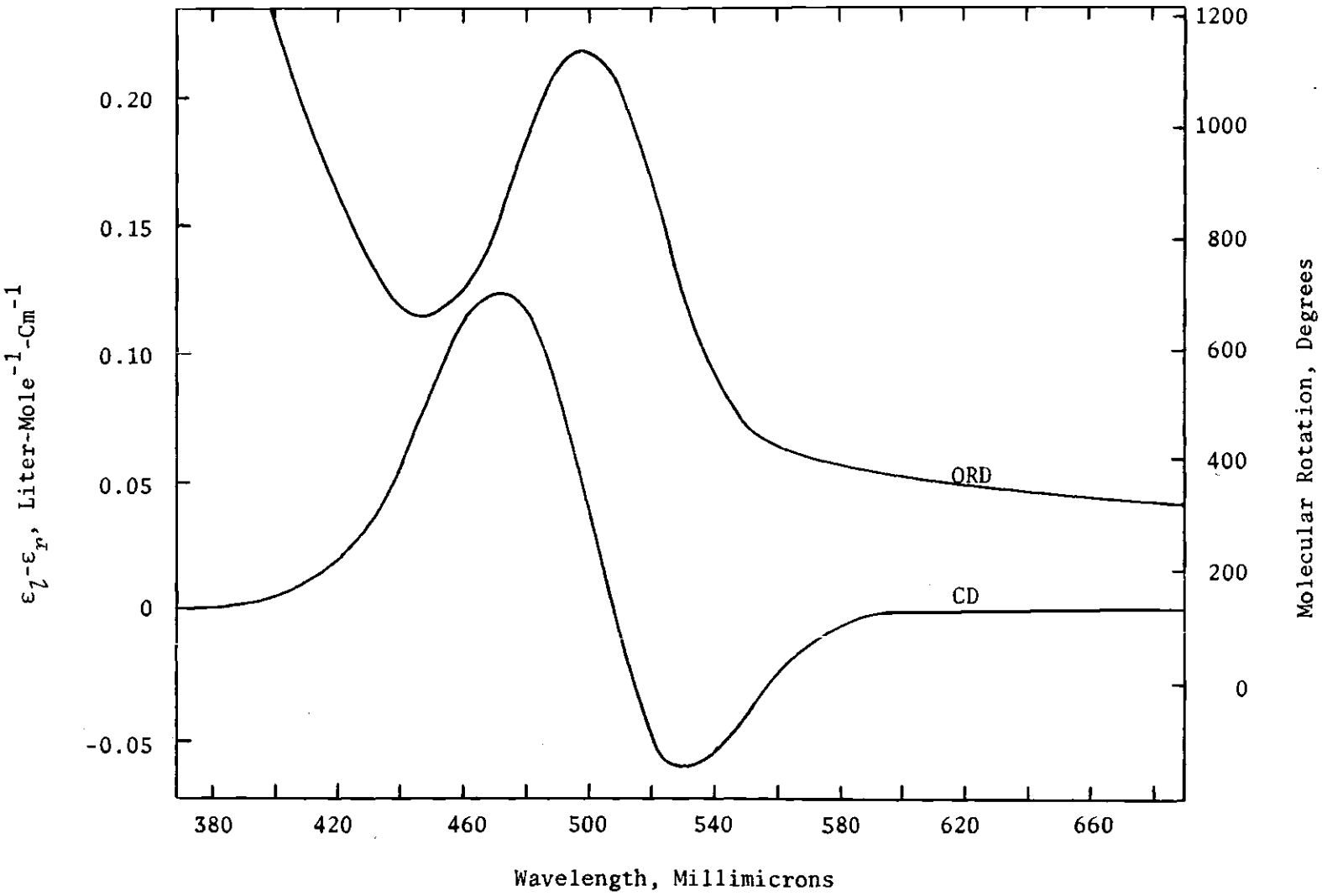

Figure 9. ORD-CD Spectra of $\Delta[Co(tn)_3]Cl_3$; Aqueous Solution

$^1A_1 \rightarrow {}^1E_a$ transition only. The CD spectra of the solution and of the single crystal are shown in Figure 10. Numerical data for the solution and crystal are given in Tables 2 and 3 respectively.

The solution CD spectrum was resolved into its component bands by the Gaussian resolution method previously mentioned. The energy separation of the component bands, as determined by this resolution, was greater than that of the corresponding bands of $\{\Lambda[Co(en)_3]Cl_3\}_2 \cdot NaCl \cdot 6H_2O$. Graphic illustration of the computer resolution of the solution CD curve for $\Delta[Co(tn)_3]^{+++}$ is shown in Figure 10. Tabulated results of the resolution are given in Table 4.

$\Lambda(+)_{589}$-*Tris*-(*d*-1,2-propanediamine)cobalt(III) Bromide

The C_3 axis of the complex ion, $\Delta[Co(l\text{-pn})_3]^{+++}$, in the hexagonal prismatic crystal, $\Delta[Co(l\text{-pn})_3]Br_3$, was found by X-ray diffraction (22) to be parallel, or nearly so, to the prismatic axis of the crystal.

The electronic absorption, ORD, and CD spectra of $\Lambda[Co(d\text{-pn})_3]Br_3$ in aqueous solution were measured. In addition, single crystal electronic absorption and CD spectra for this salt were measured with the light being propagated parallel to the prismatic axis of the crystal. With this orientation, the CD spectrum should correspond to the $^1A_1 \rightarrow {}^1E_a$ transition only. Solution ORD and CD spectra are shown in Figure 11 and the solution CD and single crystal CD spectra are shown in Figure 12. Numerical data for the solution and single crystal are given in Tables 2 and 3, respectively.

The solution CD spectrum was resolved into two Gaussian peaks as for the CD spectra of the other compounds reported. Figure 12 shows the results of this resolution, and the refined parameters are given in Table 4.

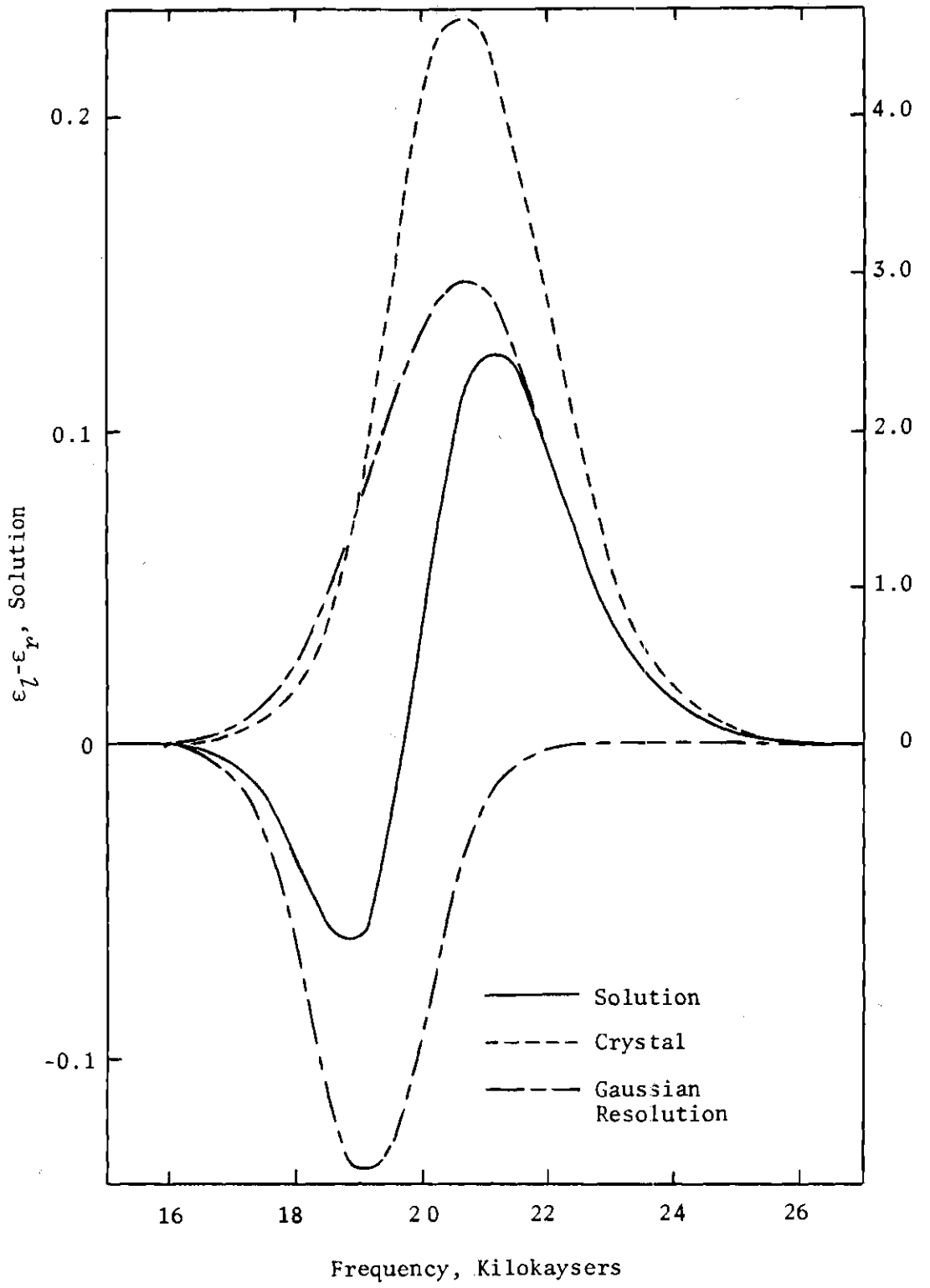

Figure 10. CD Spectra of $\Delta[Co(tn)_3]Cl_3 \cdot 4H_2O$

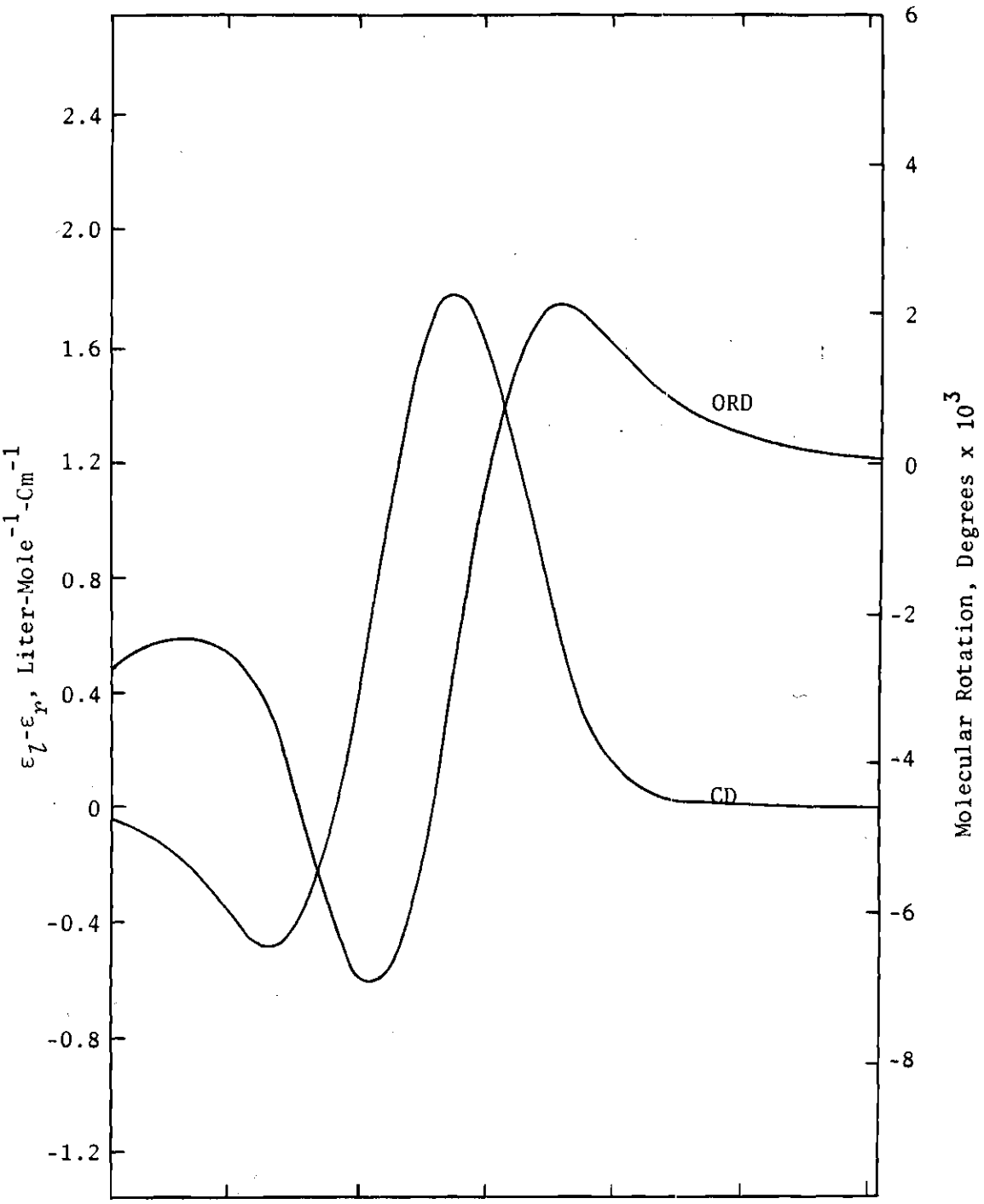

Figure 11. ORD-CD Spectra of Λ[Co(*d*-pn)$_3$]Br$_3$; Aqueous Solution

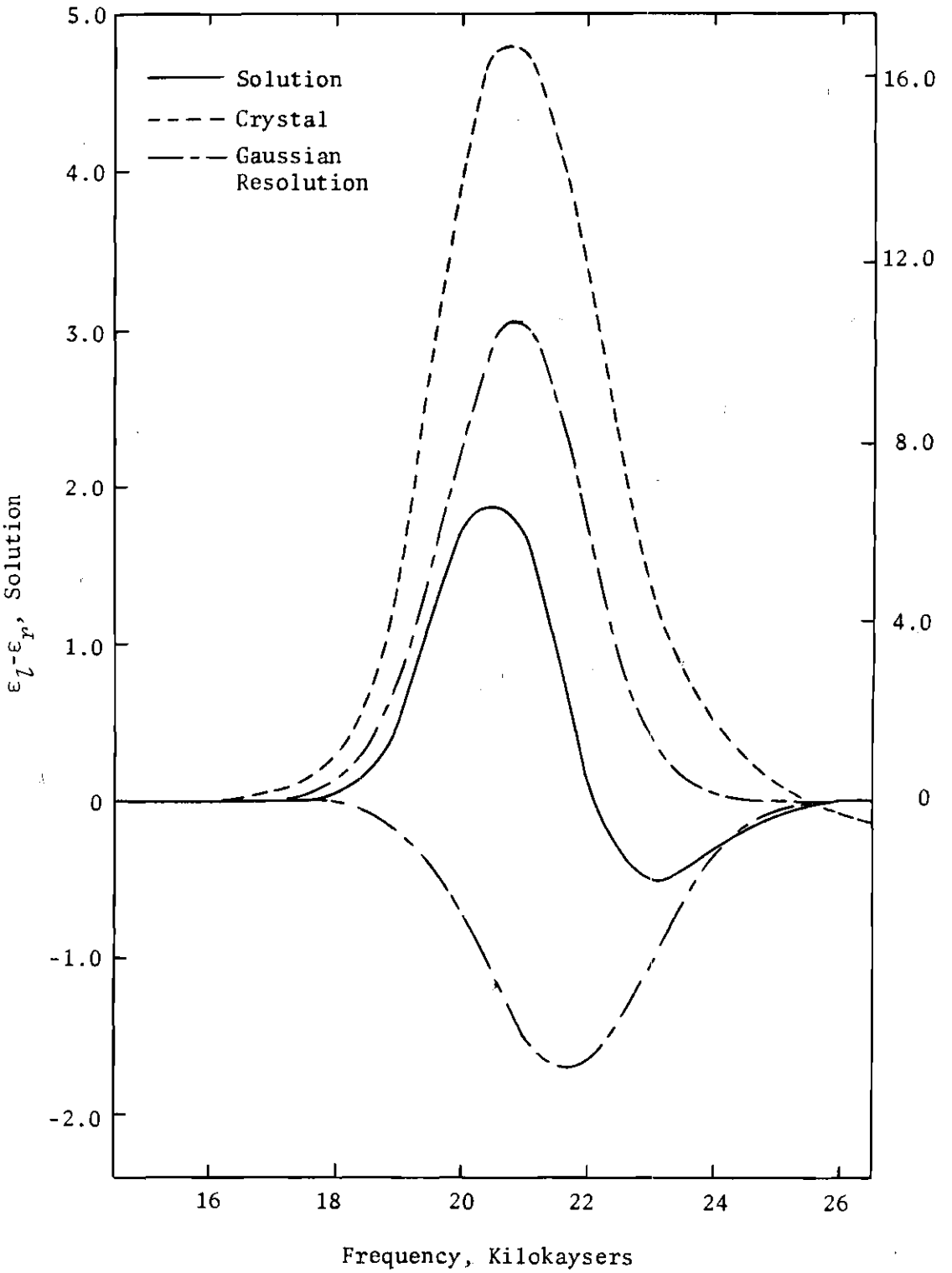

Figure 12. CD Spectra of $\Lambda[Co(d\text{-pn})_3]Br_3$

$(+)_{589}$-*Tris*-(triethylenetetramine)dicobalt(III) Chloride

Electronic absorption, ORD, and CD spectra of the salt, $(+)_{589}[Co_2(trien)_3]Cl_6$, in aqueous solution were measured. Numerical data pertaining to these measurements are given in Table 2 and the ORD and CD curves are shown in Figure 13.

The solution CD spectrum was resolved into two Gaussian peaks by the method previously mentioned in this chapter. However, since no single crystal CD spectrum was measured, it was not possible to fix the position of the peak corresponding to the $^1A_1 \rightarrow {}^1E_a$ transition as was done for the other resolutions. Therefore, all six of the parameters were varied to obtain the best fit. The results of the resolution are graphically shown in Figure 14 and the refined parameters are tabulated in Table 4.

Nuclear Magnetic Resonance Experiments

Sodium *Tris*-(ethylenediamine)cobalt(III) Chloride Hexahydrate

A sample nmr spectrum showing the quadrupolar splitting is shown in Figure 15. This spectrum was for a single crystal of $\{[Co(en)_3]Cl_3\}_2 \cdot NaCl \cdot 6H_2O$. The orientation of the crystal was such that the prismatic axis of the crystal, and thus the C_3 axis of the complex ion, $[Co(en)_3]^{+++}$, was perpendicular to the polarizing magnetic field, H_o.

The resonance positions, in kHz, of the cobalt nuclei for the various orientations of the single crystals of $\{[Co(en)_3]Cl_3\}_2 \cdot NaCl \cdot 6H_2O$ with respect to H_o are given in Tables 5 and 6. The headings in the tables are simply arbitrary labels for the component transitions.

Table 5 is a tabulation of data for rotation of the crystal (see

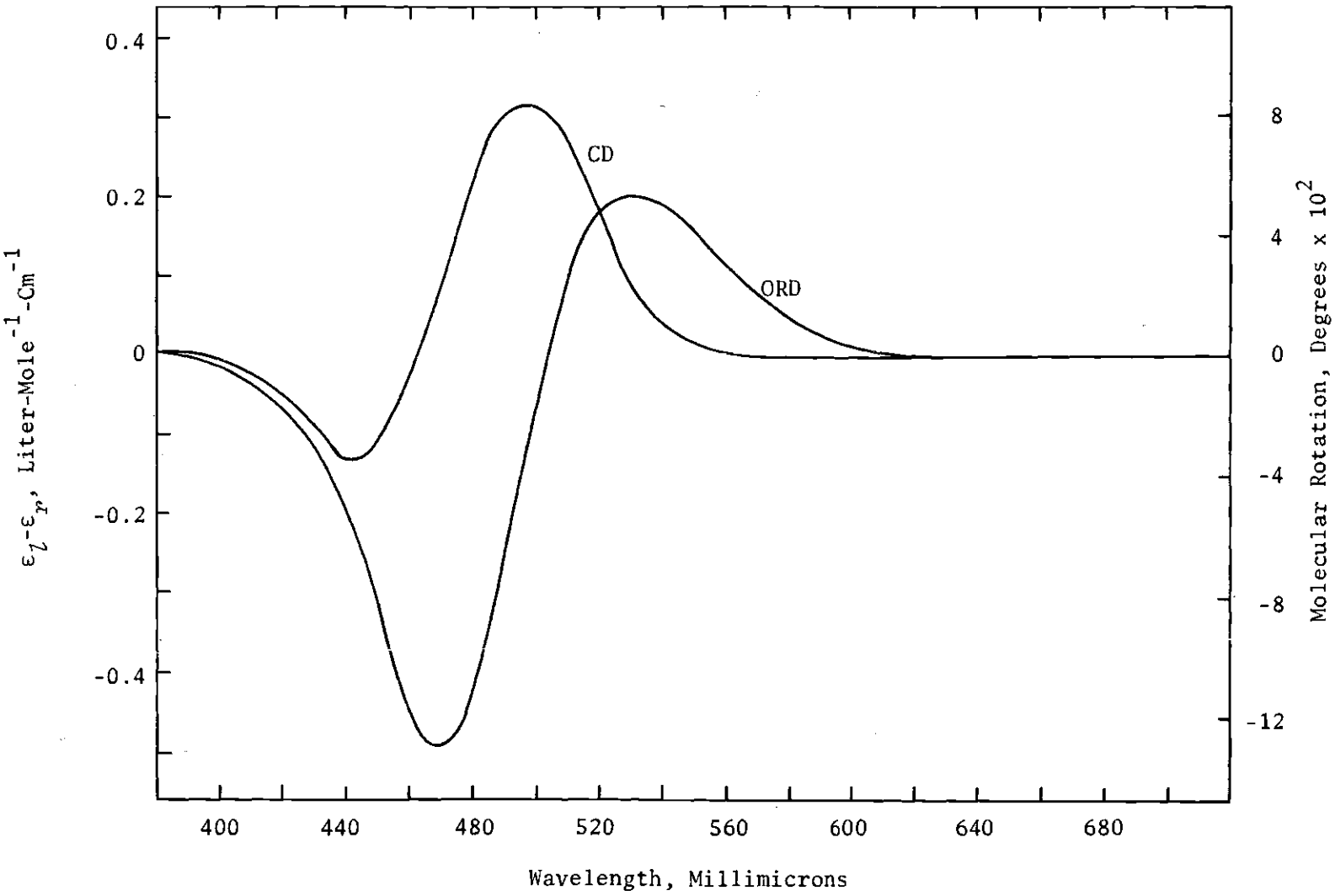

Figure 13. ORD-CD Spectra of $(+)_{589}[Co_2(trien)_3]Cl_6$; Aqueous Solution

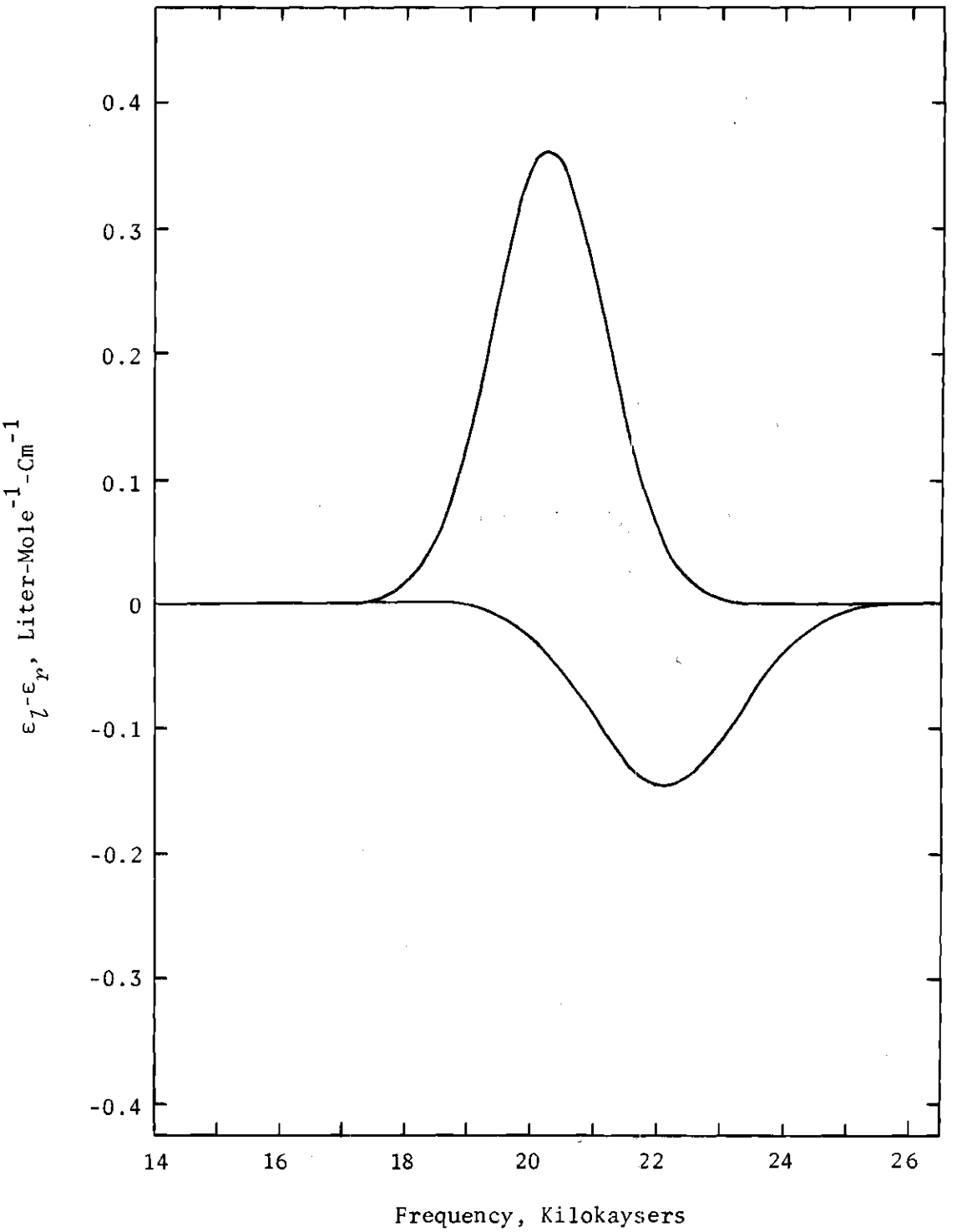

Figure 14. Gaussian Resolution of CD Spectrum of $(+)_{589}[Co_2(trien)_3]Cl_6$

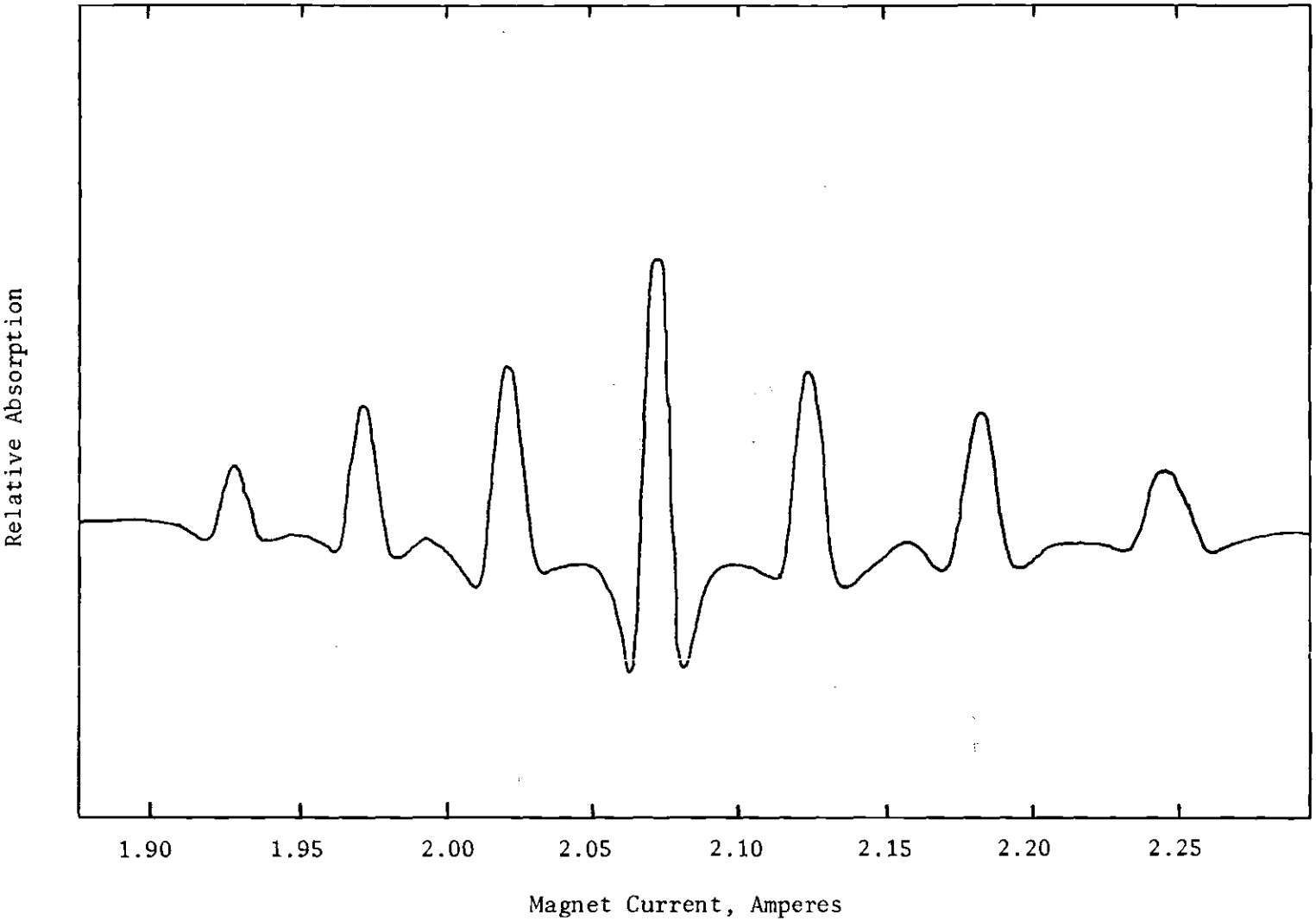

Figure 15. ^{59}Co Nuclear Magnetic Resonance Spectrum of $\{[Co(en)_3]Cl_3\}_2 \cdot NaCl \cdot 6H_2O$; Orientation: 90° From c-Axis, 0° From a-Axis

Table 5. ^{59}Co Resonances, at 14821 Gauss, for $\{[Co(en)_3]Cl_3\}_2 \cdot NaCl \cdot 6H_2O$; Rotation About the *a*-Axis.

Angle of Rotation, *r*, Degrees (±0.25°) from *c*-Axis	Resonance Positions, kHz ± 10kHz						
	ν_1	ν_2	ν_3	ν_4	ν_5	ν_6	ν_7
-5	14236	14527	14816	15085	15345	15637	15935
5	14240	14527	14806	15085	15338	15635	15935
15	14313	14570	14831	15085	15334	15596	15845
25	14466	14673	14875	15085	15292	15515	15734
35	14641	14782	14930	15085	15235	15398	15531
45	14873	14930	15000	15085	15158	15261	15319
55	15085	15085	15085	15085	15085	15085	15085
65	15296	15220	15149	15085	15013	14947	14885
75	15435	15313	15192	15085	14970	14846	14728
85	15499	15353	15209	15085	14935	14798	14661
95	15472	15345	15209	15085	14935	14798	14670
105	15430	15303	15168	15085	14965	14844	14733
115	15301	15223	15147	15085	15013	14955	14880
125	15085	15085	15085	15085	15085	15085	15085
135	14900	14950	15030	15085	15179	15290	15345
145	14677	14801	14935	15085	15225	15377	15540
155	14476	14677	14878	15085	15285	15510	15739
165	14318	14577	14834	15085	15334	15598	15865

Table 6. ^{59}Co Resonances, at 14821 Gauss, for $\{[Co(en)_3]Cl_3\}_2 \cdot NaCl \cdot 6H_2O$; Rotation About the c-Axis

Angle of Rotation, r, Degrees ($\pm 0.25^\circ$) from a-Axis	Resonance Positions, kHz ± 10kHz						
	ν_1	ν_2	ν_3	ν_4	ν_5	ν_6	ν_7
0	15494	15355	15209	15085	14945	14806	14665
10	15499	15361	15214	15085	14945	14801	14664
20	15494	15355	15214	15085	14945	14801	14656
30	15494	15355	15214	15085	14948	14806	14665
40	15499	15361	15214	15085	14948	14806	14665
50	15494	15355	15209	15085	14945	14806	14665
60	15494	15355	15214	15085	14935	14796	14661
70	15496	15356	1212	15085	14935	14796	14670
80	15494	15355	15214	15085	14945	14806	14661
90	15496	15355	15214	15085	14940	14806	14665
100	15494	15355	15214	15085	14945	14806	14670
110	15496	15350	15204	15085	14950	14816	14667
120	15494	15355	15214	15085	14945	14806	14668
130	15496	15355	15219	15085	14945	14811	14670
140	15499	15355	15209	15085	14945	14806	14665
150	15496	15355	15209	15085	14945	14806	14663
160	15495	15355	15212	15085	14945	14801	14661
170	15499	15353	15209	15085	14940	14806	14665

Figure 4) about the a-axis of the crystal. In turn, this corresponds to rotation of H_o about an axis perpendicular to the C_3 axis of the complex ion, $[Co(en)_3]^{+++}$. The angle r refers to the angle between the magnetic field direction and the reference axis of the crystal. Note that r is not the same as α where α is the angle between the reference axis and the projection of the z-principal axis of the electric field gradient on the rotation plane.

Table 6 is a tabulation of data for rotation of the crystal about its c-axis (see Figure 4). This corresponds to rotation of H_o about an axis parallel to the C_3 axis of $[Co(en)_3]^{+++}$. One-half of a rotation is sufficient since the pattern repeats every 180°.

Graphic illustration of the variation of the quadrupolar splitting of the nmr spectra as a function of orientation is shown in Figure 16, which is a plot of a portion of the data of Tables 5 and 6. That portion of the plot where $\theta = 90°$ corresponds to rotation about the crystallographic c-axis (or the z-axis of the electric field gradient). That portion of the plot where $\phi = 90°$ corresponds to rotation about the crystallographic a-axis (or the y-axis of the electric field gradient). The closed circles represent experimental data and the solid lines are calculated curves. The calculated curves are first-order perturbation calculations (33) based on the experimentally determined values of the quadrupole coupling constant of the cobalt nuclei and the orientation of the cobalt nuclei with respect to the magnetic field. The equation used for this calculation was,

$$\Delta\nu = C_3(2m-1)(3\cos^2\theta-1)/4, \qquad (42)$$

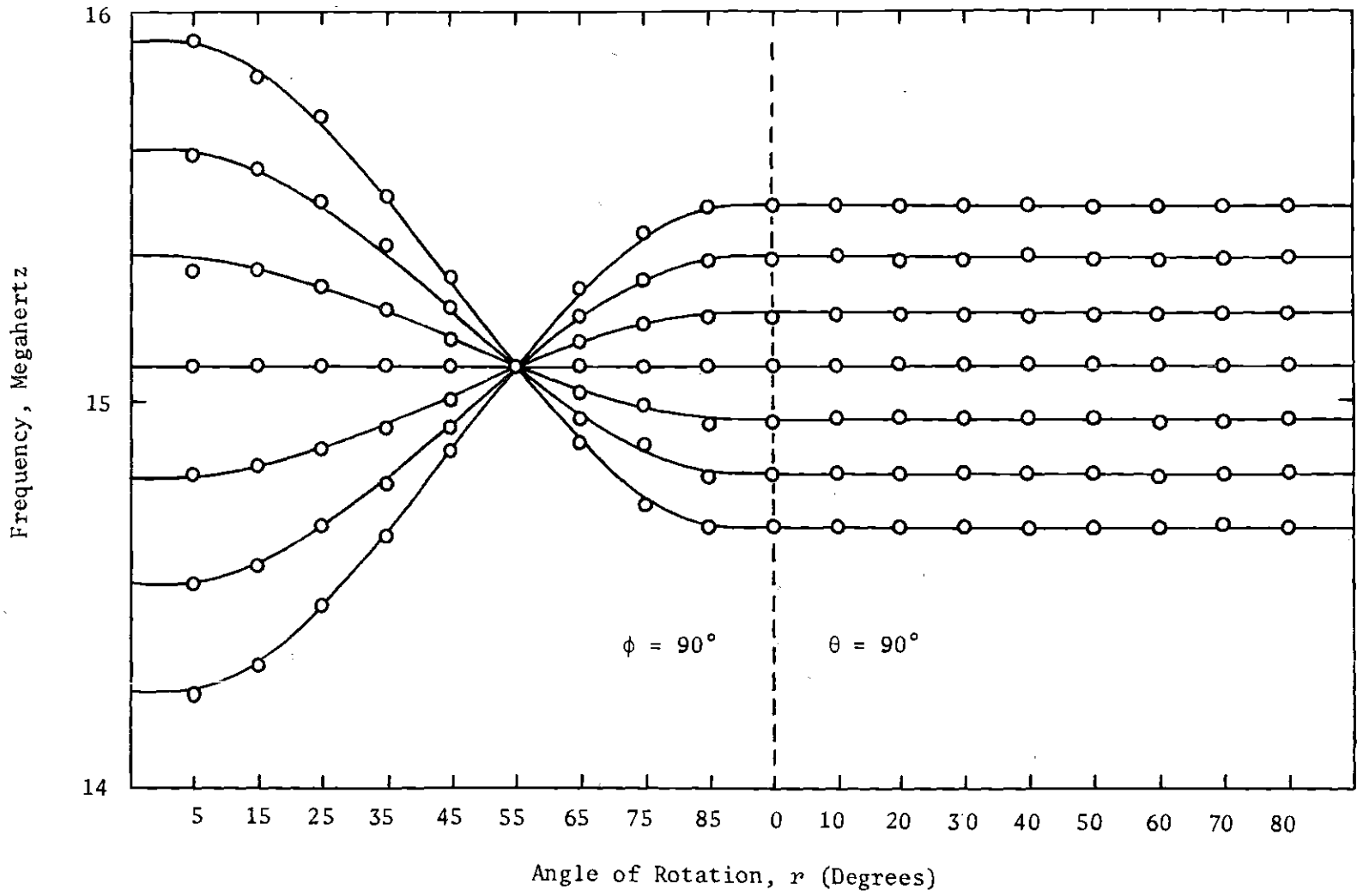

Figure 16. Variation of Quadrupolar Splitting in $\{[Co(en)_3]Cl_3\}_2 \cdot NaCl \cdot 6H_2O$ With Rotation About Axes of the Electric Field Gradient

where $\Delta\nu$ is the frequency separation of a line from the unperturbed Larmor frequency, ν_o, C_3 is defined as in Chapter II, m is the value of the magnetic quantum number of the perturbed level, and θ is the angle between the principal axis of the electric field gradient and the magnetic field direction.

Table 7 gives the results of the calculations of the nuclear parameters from the experimental data by the method outlined in Chapter II.

Tris-(1,3-propanediamine)cobalt(III) Salts

A sketch of the crystal habit of the compound, $[Co(tn)_3](NO_3)_3$ is shown in Figure 17. The resonances in kHz of the cobalt nuclei for the various orientations of the crystal with respect to H_o are given in Table 8. These data were obtained for rotation of the crystal about the crystallographic *b*-axis. Graphic illustration of these data is given in Figure 18. These data indicated that the C_3 axis of the complex ion, $[Co(tn)_3]^{+++}$, was not parallel to any of the three crystallographic axes. The principal axis of the electric field gradient, and thus the three-fold axis of the complex ion, is in a plane located approximately 54° from the crystallographic *b*-axis and not along either the crystallographic *a*-axis or *c*-axis. The nuclear parameters are tabulated in Table 7.

It was unfortunate that this crystal did not have a crystallographic face perpendicular to the principal axis of the electric field gradient since it was very stable and well-formed crystals were easily obtained. Had such a face been found, the crystals would probably have been very good for use in the single crystal CD measurements. However, the nmr data obtained appear to be very good and a value for the quadrupole

Table 7. Nuclear Parameters for the Amine Complexes of Cobalt(III)

Compound	$\lvert e^2Qq/h \rvert$ (MHz)	η
$\{[Co(en)_3]Cl_3\}_2 \cdot NaCl \cdot 6H_2O$	3.92 ± 0.02	0
$[Co(tn)_3](NO_3)_3$	6.19 ± 0.02	0
$[Co(tn)_3]Cl_3 \cdot 4H_2O$	6.19 ± 0.02	0
$\Lambda[Co(d\text{-}pn)_3]Br_3$	4.79 ± 0.04	0
$(+)_{589}[Co_2(trien)_3](NO_3)_6 \cdot 6H_2O$		
Pattern Number One	5.35 ± 0.04	0
Pattern Number Two	5.35 ± 0.04	0

Table 8. ^{59}Co Resonances, at 14821 Gauss, for $[Co(tn)_3](NO_3)_3$; Rotation About the *b*-Axis.

Angle of Rotation, *r*, Degrees (±0.25°) from *a*-Axis	Resonance Positions, kHz ± 10kHz						
	ν_1	ν_2	ν_3	ν_4	ν_5	ν_6	ν_7
-5	15276	15220	15150	15085	15014	14948	14894
5	15375	15273	15181	15085	14988	14895	14795
15	15530	15380	15232	15085	14937	14789	14641
25	15635	15463	15266	15085	14900	14709	14536
35	15665	15470	15278	15085	14892	14699	14506
45	15705	15497	15291	15085	14879	14669	14463
55	15735	15508	15294	15085	14873	14662	14435
65	15700	15493	15285	15085	14885	14677	14469
75	15624	15442	15265	15085	14905	14727	14546
85	15565	15405	15245	15085	14925	14765	14605
95	15385	15288	15187	15085	14984	14875	14784
105	15278	15222	15154	15085	15016	14948	14892

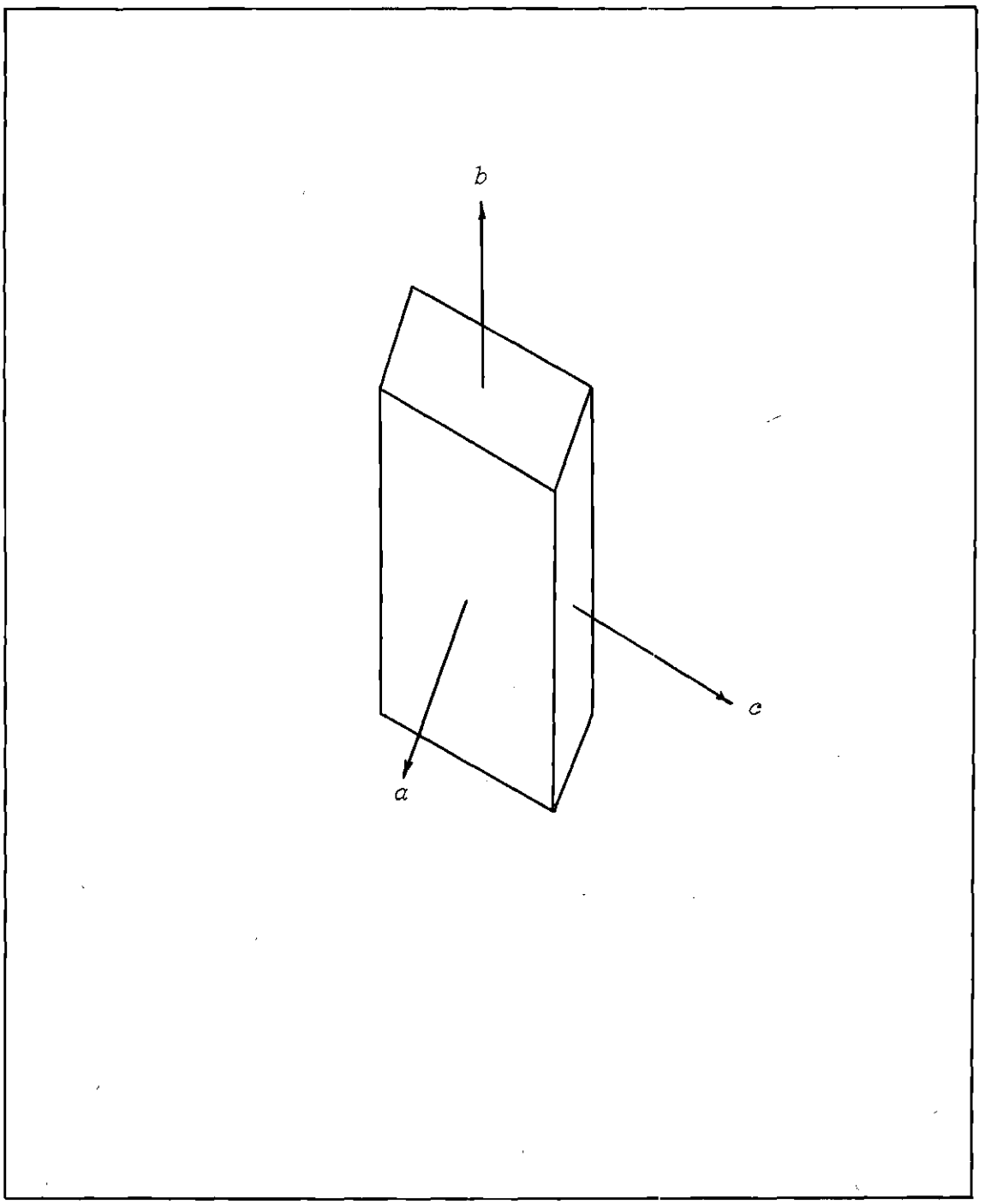

Figure 17. Crystalline Habit of $[Co(tn)_3](NO_3)_3$

coupling constant was obtained.

The resonances in kHz of the cobalt nuclei for various orientations of a single crystal of $[Co(tn)_3]Cl_3 \cdot 4H_2O$ with respect to H_o are given in Table 9. These data were for rotation of the crystal about the crystallographic *a*-axis (see Figure 4). A complete rotation pattern for this crystal was not obtained, because the tube containing the crystal was cracked and the crystal dehydrated and turned to a powder. The numbers in parentheses are calculated positions based on the splittings observed for the other peaks. The outermost peaks were very broad and no attempt was made to locate their positions experimentally. The spectra that were obtained were especially useful, however, because when combined with the nmr data for the crystal, $[Co(tn)_3](NO_3)_3$, determination of the location of the principal axis of the electric field gradient, and thus the C_3 axis of the complex ion, $[Co(tn)_3]^{+++}$, with respect to the crystallographic axes of $[Co(tn)_3]Cl_3 \cdot 4H_2O$ was possible. The C_3 axis was found to be parallel to the crystallographic *b*-axis.

The nmr data for $[Co(tn)_3]Cl_3 \cdot 4H_2O$ was not used in the determination of the quadrupole coupling constant. However, the value of the coupling constant calculated from the $[Co(tn)_3](NO_3)_3$ data was used to calculate theoretical curves (by means of Eq. [42]) for the splitting in the spectra of $[Co(tn)_3]Cl_3 \cdot 4H_2O$. The results of this calculation are the solid lines in Figure 19. The closed circles are the experimentally determined resonance frequencies. The cross marks are calculated positions. The very good fit of the data for $[Co(tn)_3]Cl_3 \cdot 4H_2O$ to these theoretical curves was the basis for the determination that the electric field gradient was parallel to the crystallographic *b*-axis.

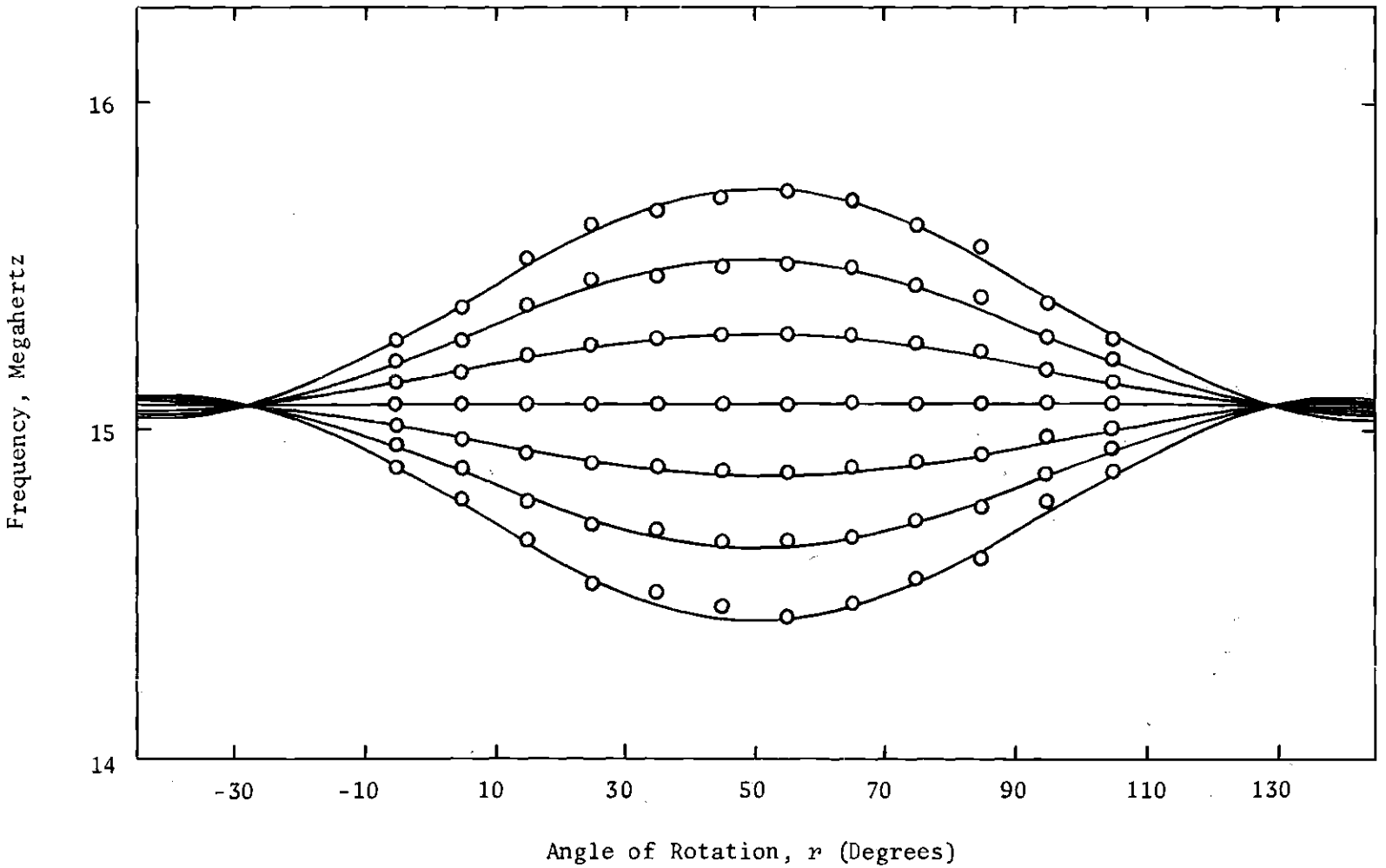

Figure 18. Variation of Quadrupolar Splitting in $[Co(tn)_3](NO_3)_3$ With Rotation About the *b*-Axis

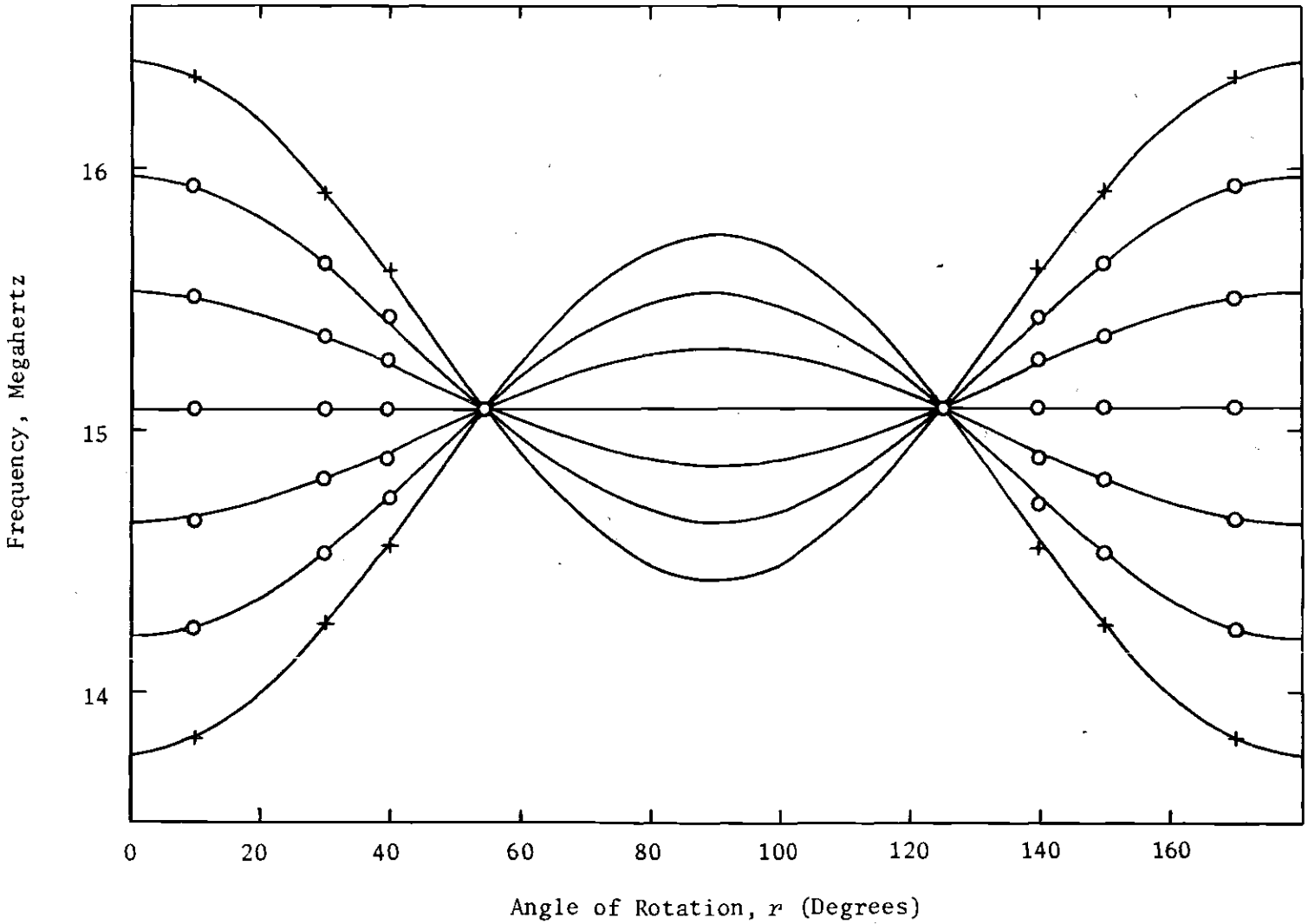

Figure 19. Variation of Quadrupolar Splitting in $[Co(tn)_3]Cl_3 \cdot 4H_2O$ With Rotation About the *a*-Axis

Table 9. ^{59}Co Resonances, at 14821 Gauss, for $[Co(tn)_3]Cl_3 \cdot 4H_2O$; Rotation About the *a*-Axis.

Angle of Rotation, *r*, Degrees (±0.250°) from *b*-Axis	Resonance Positions, kHz ± 10kHz						
	ν_1	ν_2	ν_3	ν_4	ν_5	ν_6	ν_7
0	(13760)	14202	14643	15085	15527	15968	(16410)
10	(13820)	14242	14663	15085	15507	15928	(16350)
30	(14257)	14533	14809	15085	15361	15637	(15913)
40	(14581)	14749	14917	15085	15253	15421	(15589)
50	(14926)	14979	15032	15085	15138	15191	(15244)
55	15085	15085	15085	15085	15085	15085	15085
125	15085	15085	15085	15085	15085	15085	15085
130	(14926)	14979	15032	15085	15138	15191	(15244)
140	(14581)	14749	14917	15085	15253	15421	(15589)
150	(14257)	14533	14809	15085	15361	15637	(15913)
170	(13820)	14242	14663	15085	15507	15928	(16350)
180	(13760)	14202	14643	15085	15527	15965	(16410)

The determination of principal axis position allowed the single crystal CD measurements to be made since it was necessary to propagate light parallel to the three-fold axis of the complex ion, $\Delta[Co(tn)_3]^{+++}$, in order to measure the pure spectrum corresponding to the $^1A_1 \rightarrow {}^1E_a$ transition

$\Lambda(+)_{589}$*Tris*-(*d*-1,2-propanediamine)cobalt(III) Bromide

A single crystal of $\Lambda[Co(d\text{-pn})_3]Br_3$ of suitable size for single crystal nmr studies could not be grown. However, it was possible to obtain an nmr spectrum of a powder of this material. The precision of this experiment was somewhat lower than for the single crystal nmr studies, but reasonably good spectra were obtained and the value of the quadrupole coupling constant of ^{59}Co in this compound was calculated by the method given in Chapter II. The asymmetry parameter for this compound was zero since the crystal had hexagonal symmetry as determined by an X-ray study (22). The experimental data are given in Table 10, and the quadrupole coupling constant obtained from the nmr data for $\Lambda[Co(d\text{-pn})_3]Br_3$ is given in table 7.

Table 10. ^{59}Co Resonances, at 14821 Gauss, for $\Lambda[Co(d\text{-pn})_3]Br_3$ Powder.

Resonance Positions, kHz ±25kHz

ν_1	ν_2	ν_3	ν_4	ν_5	ν_6	ν_7
(14574)	14744	14914	15085	15256	15426	(15596)

Tris-(triethylenetetramine)dicobalt(III) Nitrate Hexahydrate

A drawing of a crystal of this material along with its rotation axes is shown in Figure 20. This drawing is given to establish reference axes only. As may be seen by the drawing, the habit of the crystal was not simple and it was not supposed that all the crystal faces had developed.

Tables 11 and 12 are tabulations of data for rotation about the crystallographic *c*-axis. The spectra for this compound consisted of thirteen resonance lines. Since ^{59}Co has a nuclear spin of 7/2 and quadrupolar splitting is present, seven resonance lines should be observed for each unique cobalt nucleus. Thus, two unique cobalt nuclei sites exist in the crystalline lattice. The center line is common to both nuclei.

Figure 21 is a plot of the data of Table 11 which is a rotation pattern for one of the unique cobalt nuclei. Table 12 contains the data which is a rotation pattern for the second unique cobalt nucleus. The numbers in parentheses in Tables 11 and 12 are calculated resonance positions based on the average splitting of the other peaks. These calculated positions are indicated by crosses in Figure 21.

The quadrupole coupling constant was found to be the same for each of the patterns. The values of the coupling constant and the asymmetry parameter are given in Table 7.

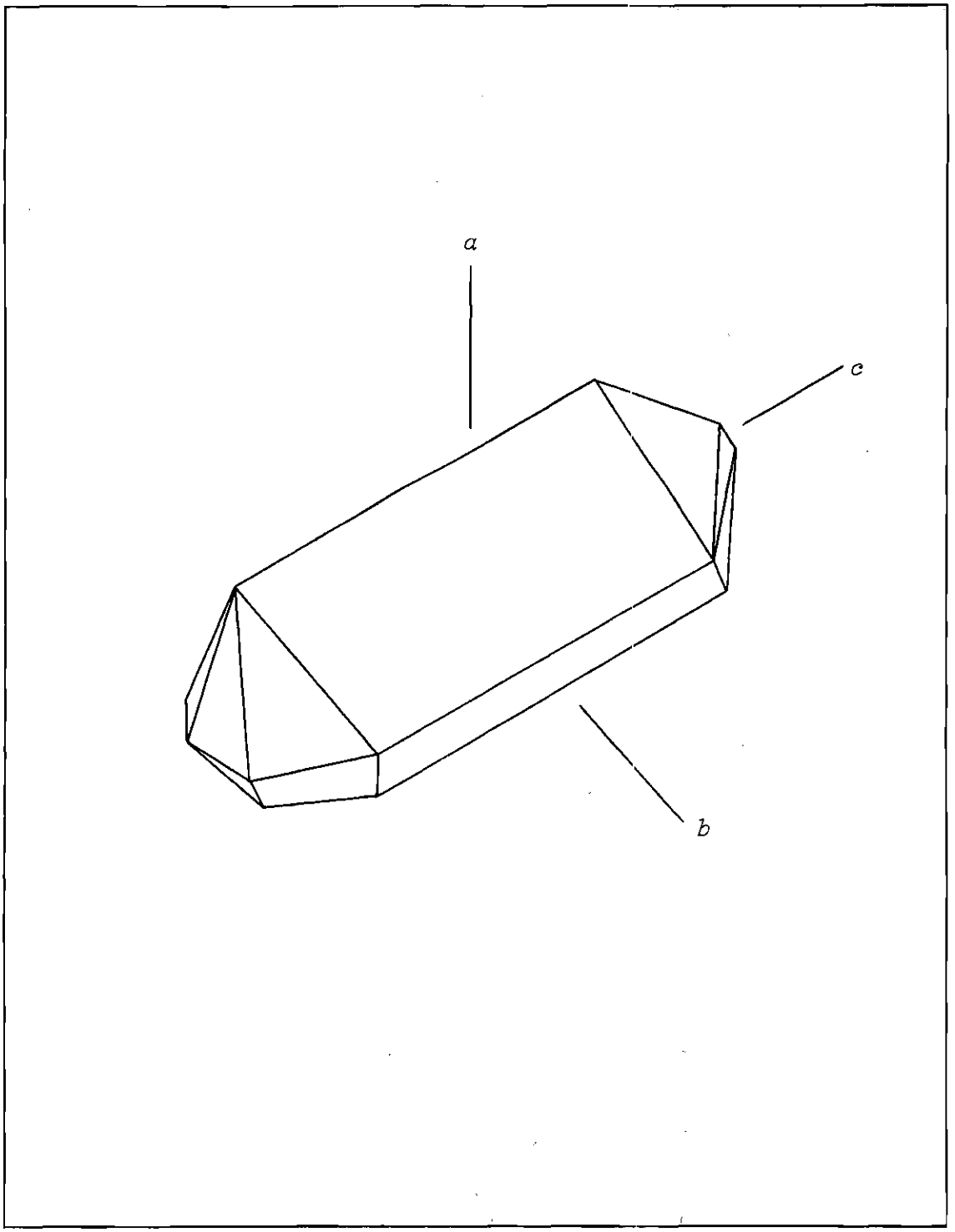

Figure 20. Crystalline Habit of $[Co_2(trien)_3](NO_3)_6 \cdot 6H_2O$

Table 11. ^{59}Co Resonances, at 14821 Gauss, for $[Co_2(trien)_3](NO_3)_6 \cdot 6H_2O$; Rotation About the *c*-Axis; Pattern Number One.

Angle of Rotation, *r*, Degrees (±0.250°) from *a*-Axis	Resonance Positions, kHz ± 20kHz						
	ν_1	ν_2	ν_3	ν_4	ν_5	ν_6	ν_7
10	(14972)	(15013)	15054	15085	15128	15176	(15217)
20	14955	14995	(15043)	15085	15125	15160	15211
30	14938	14972	15040	15085	15133	15179	15238
40	(14883)	14955	15015	15085	15160	15238	15316
50	14741	14880	14957	15085	15198	(15312)	(15426)
60	(14658)	(14800)	(14942)	15085	15233	15370	(15512)
80	(14578)	14750	14915	15085	15265	15428	15612
100	14510	14700	14884	15085	15267	15467	15660
130	(14609)	14770	14926	15085	15244	15415	(15576)
160	14899	(14950)	15012	15085	15143	(15206)	(15268)
170	14955	15005	(15044)	15085	15123	(15164)	15195

Table 12. ^{59}Co Resonances, at 14821 Gauss, for $[Co(trien)_2]_3(NO_3)_6 \cdot 6H_2O$; Rotation About the c-Axis; Pattern Number Two.

Angle of Rotation, r, Degrees ($\pm 0.250°$) from a-Axis	Resonance Positions, kHz ± 20kHz						
	ν_1	ν_2	ν_3	ν_4	ν_5	ν_6	ν_7
0	(14510)	(14700)	14904	15085	(15275)	15486	15665
10	(14555)	(14735)	14910	15085	15260	15430	(15610)
20	14662	(14810)	14955	15085	15211	(15365)	15498
30	(14835)	14923	15000	15085	15164	15240	(15340)
40	15040	(15060)	(15072)	15085	15100	15110	15128
50	15254	15198	15146	15085	(15020)	14957	14880
60	(15480)	15370	15219	15085	14957	14842	(14700)
70	(15645)	15460	15370	15085	14902	(14710)	(14520)
80	(15760)	15630	15316	15085	14860	(14640)	(14410)
90	(15795)	(15660)	15306	15085	14850	(14600)	(14370)
120	(15470)	15345	(15220)	15085	14948	14844	(14695)
130	15244	15203	15146	15085	15022	14978	14926
140	15025	(15045)	(15060)	15085	15100	15113	15128
150	14818	(14920)	15000	15085	15170	15261	(15330)
170	(14560)	(14730)	14897	15085	15260	15430	15615

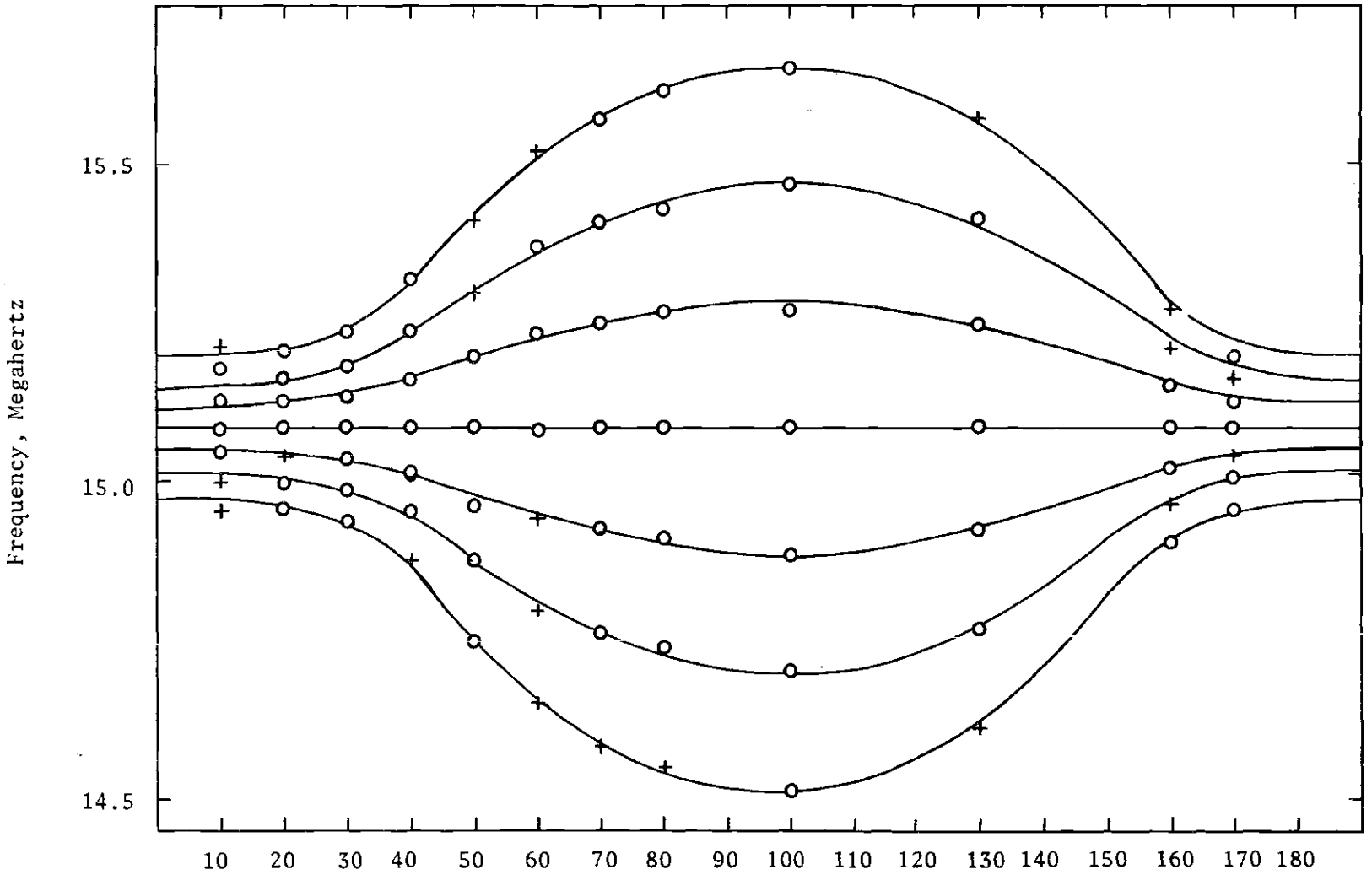

Figure 21. Variation of Quadrupolar Splitting in $[Co_2(trien)_3](NO_3)_6 \cdot 6H_2O$ With Rotation About the c-Axis

CHAPTER V

DISCUSSION AND CONCLUSIONS

The ultimate goals of the study of ORD and CD spectra of transition metal complexes are generally (48,52) recognized to be the determination of a relation between the features of the ORD and/or CD curves and the absolute configuration of the complex ions, and the mechanism of interaction of light with the optically active medium. To accomplish these objectives, experiments must be performed to determine absolute configurations and ORD and CD studies must then be made.

The determination of absolute configurations may be accomplished by X-ray studies. However, as mentioned previously, very few absolute configurations have been determined by X-ray work, and only for $\Lambda[Co(en)_3]^{+++}$ has the geometry been accurately determined (21). Accurate geometries seem to be necessary prerequisites for construction of usable theoretical models for calculation of the optical activity.

This work was initiated with the hope of determining the appropriate model of those proposed for optical activity. It will subsequently be illustrated that none of the proposed models is suitable for a complete explanation of the experimental results. However, the model of Karipides and Piper (15) was found to be qualitatively correct.

Since deviations of the complex ions from octahedral symmetry have been commonly suggested as possible sources of optical activity, these distortions were calculated on the basis of the X-ray results

(19-23). In particular, deviations of the values of the polar and the azimuthal angles from the values in an octahedron were calculated. These angles were defined in Chapter II (the values of the polar and azimuthal angles in an octahedron are, respectively, 54.7° and 60°). The results of these calculations are summarized in Table 13. In addition, the average values of the N-Co-N angle of a chelate ring in each of the complex ions is given in Table 13.

An analysis of the correspondence between various models and the experimental results may now be made. Emphasis here will be placed on qualitative predictions of the models with the notion that if qualitative correctness is attained, refinement would probably result in better quantitative predictions. A more detailed discussion of the models may be found in Chapter II.

According to the ionic model, trigonal splitting arises due to a distortion of the complex ion along the three-fold axis. Rotational strength is assumed to arise from azimuthal distortions. The results of the calculations of the distortions of the complex ions from octahedral symmetry (calculations of the distortions were made on the basis of the known crystal structures) are given in Table 13. In the ionic model, compression along the C_3 axis should result in a negative value of the trigonal splitting, i.e., $\nu_E - \nu_A < 0$. Azimuthal contraction of Λ-type ion (or azimuthal expansion of a Δ-type ion), according to the ionic model, should yield an A_2 component of positive rotational strength, and an E_a component of equal magnitude but opposite sign.

It would seem as though the $\Lambda[Co(en)_3]^{+++}$ ion is characterized by a compression along the C_3 axis and a contraction of the azimuthal angle.

Table 13. Distortions of the Complex Ions

Compound	∠NCoN	Polar Distortion	Azimuthal Distortion
$\{\Lambda[Co(en)_3]Cl_3\}_2 \cdot NaCl \cdot 6H_2O$	87.4°	-0.98°	-6.6°
$\Lambda[Co(en)_3]Br_3 \cdot H_2O$	87.4°	+1.17°	+0.33°
$\Lambda[Co(en)_3]Cl_3 \cdot H_2O$	85.3°	+1.70°	-5°
$\Lambda[Co(tn)_3]Br_3 \cdot H_2O$	94.5°	-2.13°	+2.4°
$\Delta[Co(l\text{-}pn)_3]Br_3$	86.5°	+1.47° (N_1) -0.83° (N_2)	-5.4°

As may be noted from Table 13, however, the data for compounds that contain $\Lambda[Co(en)_3]^{+++}$ indicate widely different distortions. For example, in $\Lambda[Co(en)_3]Br_3 \cdot H_2O$, the complex ion is reported to be almost exactly octahedral. However, for $\{\Lambda[Co(en)_3]Cl_3\}_2 \cdot NaCl \cdot 6H_2O$ and for $\Lambda[Co(en)_3]Cl_3 \cdot H_2O$, deviations from the octahedral disposition are significant. In those compounds in which distortions are significant, the polar distortions are opposite in sign. For the mixed crystal with NaCl, there is an apparent elongation along the C_3 axis, and for the chloride monohydrate, there is an apparent compression along the C_3 axis. The most accurate geometry of $\Lambda[Co(en)_3]^{+++}$ is that established for the ion in the chloride monohydrate (21). This determination is the only one in which the expressed purpose was an accurate determination of geometry.

If we assume a compression along the C_3 axis, the ionic model prediction would be a negative trigonal splitting ($\nu_E - \nu_A < 0$) and an A_2 component of positive rotational strength equal in magnitude but opposite in sign to the E_a component. The experimental results verify the prediction of the positions of the component bands, but do not agree with the predictions of signs and magnitudes of the rotational strengths of these bands. The E_a component has a positive rotational strength of much greater magnitude than the negatively rotating A_2 component.

For $\Lambda[Co(d\text{-pn})_3]^{+++}$, there appears to be a net compression along the C_3 axis of the complex ion and a contraction of the azimuthal angle. Thus, the signs of the distortions are identical to those in $\Lambda[Co(en)_3]^{+++}$. The ionic model predictions would be a positive rotational strength A_2 component at the shorter wavelength and a negative rotational strength E_a component at the longer wavelength. Agreement is obtained

with the positions of the component bands but not with the signs of the rotational strengths. Also, the E_a component has a much greater magnitude than the A_2 component which is contrary to the prediction of equal magnitudes. Thus, the results here are the same as for $\Lambda[Co(en)_3]^{+++}$.

The only ion (of those studied) that appears to have a definite elongation along the C_3 axis is $\Delta[Co(tn)_3]^{+++}$. This ion is also characterized by an azimuthal expansion. Thus, the distortions of this ion are opposite in sign to those of $\Lambda[Co(en)_3]^{+++}$ and $\Lambda[Co(d\text{-pn})_3]^{+++}$. The ionic model predictions are for a long wavelength A_2 component of positive rotational strength and a short wavelength E_a component of negative rotattional strength and for equal magnitudes of the rotational strengths. The prediction of relative positions of the component bands is in agreement with experiment. However, the predictions of signs and relative magnitudes of the rotational strengths do not agree with experiment.

For the compounds discussed above, it is possible that the ions are not distorted sufficiently to decide on the signs of the distortions (along the C_3 axis) from the X-ray results. However, from the nmr results (the magnitudes of the quadrupole coupling constants), the electronic distortions along the C_3 axes of the complex ions vary in the order, $\Delta[Co(tn)_3]^{+++} > \Lambda[Co(d\text{-pn})_3]^{+++} > \Lambda[Co(en)_3]^{+++}$. The nmr results are probably more reliable measures of the absolute values of the axial distortions than the X-ray results. The quadrupole coupling constants are indicative of actual electronic distortions and are accurate to about ±1%. The geometric distortions as determined by X-ray studies are of the same order of magnitude as the estimated standard deviations of the atomic positions. For those ions for which we have the most reliable

X-ray data ($\Lambda[Co(tn)_3]^{+++}$ and $\Lambda[Co(en)_3]^{+++}$), the indications are clearly that the polar distortions are opposite in sign and greater in magnitude for $\Delta[Co(tn)_3]^{+++}$. On the basis of the similarities in the ORD and CD spectra of $\Lambda[Co(en)_3]^{+++}$ and $\Lambda[Co(d\text{-pn})_3]^{+++}$, it may be concluded that the signs of the axial distortions are identical and are opposite to the sign of the axial distortion of $\Delta[Co(tn)_3]^{+++}$. Namely, the ions, $\Lambda[Co(en)_3]^{+++}$ and $\Lambda[Co(d\text{-pn})_3]^{+++}$ are compressed along the C_3 axes and $\Delta[Co(tn)_3]^{+++}$ is elongated along the C_3 axis.

The magnitude of the trigonal splittings (as determined by the Gaussian resolutions of the CD spectra) varied in the same order as the magnitudes of the axial distortions. Thus, the conclusions based on the nmr results are substantiated by the trigonal splittings. That is, the greater the axial distortion of an ion, the greater the values of the coupling constant and the trigonal splitting.

Karipides and Piper (15), on the basis of their moecular orbital model, gave the same predictions of signs of trigonal splittings as they did in their ionic model. Namely, a compression of the octahedron along a C_3 axis results in a negative trigonal splitting. It is tentatively suggested that for azimuthal expansion of a Λ-type ion (or azimuthal contraction of a Δ-type ion), the complex ion will have a positive rotational strength A_2 component. They noted that their model did not allow calculation of the sign of the optical activity with certainty. The tentative suggestion for sign predictions was made on the basis of the known (17) signs of rotational strengths of the component bands of $\Lambda[Co(en)_3]^{+++}$. Our data are in agreement with the predictions of relative positions of the component bands and the signs of the rotational strengths.

However, their model predicts equal magnitudes of rotational strengths of the component bands, which is at variance with the experimental results. However, the E_a component may be made more positive or more negative by the differences in q_o and q_2 (the q's were defined in Chapter II).

Of especial importance in the foregoing discussion is that an azimuthal expansion in a Δ-type ion is equivalent to an azimuthal contraction in a Λ-type ion, because their calculated signs of the optical activity depend only on the position of the six ligand atoms of the first coordination sphere.

Liehr's (16) misdirected orbitals model predicts that the signs of the rotational strengths should be determined only by the chirality of the complex. This prediction does not agree with the experimental results of this work. The ions, $\Lambda[Co(en)_3]^{+++}$ and $\Lambda[Co(d\text{-pn})_3]^{+++}$, exhibit Cotton effects for the component CD bands of the same signs as the Cotton effects for the component CD bands of $\Delta[Co(tn)_3]^{+++}$. He also suggested that the magnitude of the rotational strength should be proportional to the value of his angle of cant. If this supposition were correct, a definite relationship between the rotational strengths and the values of the quadrupole coupling constants should exist. Namely, the greater the value of the coupling constant, the greater should be the value of the rotational strength. Clearly, this is not the case since the ion, $\Delta[Co(tn)_3]^{+++}$, with the greatest value of the coupling constant has the lowest rotational strength.

Liehr further suggested that reasonable values of the angle of cant would be ≈15° to generate significant rotation. This large an angle

would presumably lead to much larger quadrupole coupling constants than were observed. This would also destroy the observed correlation between the coupling constant (which measures the electronic distortion) and the geometric distortion.

The model presented by McCaffery and Mason (17), in which rotatory power is acquired by mixing with ligand or charge-transfer transitions, suggests relating the chirality of the enantiomers giving an E_a component with a positive rotational strength to that of $\Lambda[Co(en)_3]^{+++}$. This suggestion is not valid in the case of $\Delta[Co(tn)_3]^{+++}$ which has an E_a component with a positive rotational strength. Other than this discrepancy, though, little can be said in a comparison of the present experimental results and their theoretical model. However, extensive mixing of this type would tend to destroy the relationship between the trigonal splitting and quadrupole coupling constant.

Of particular interest is the inability of any of the theories to explain the "ring-size-effect" that is observed in the six-membered chelate ring complex. This effect seems to be manifest in a large decrease in rotational strength of the six-membered chelate ring complex as compared to the five-membered chelate ring complexes. Woldbye (53) discussed this effect on an empirical basis, but apparently none of the theoretical discussions attempts to explain it.

For the models discussed here, the assumptions were that trigonal splittings are small and that the CD curves are essentially residual wing absorptions. That is, the activity may be thought of as the relatively small residual activity left by the partial cancellation of two large, opposed rotational strengths. Indications from this work are that this

is not the case. The splittings appear to be considerably greater than had been calculated (54,55) on the basis of single crystal absorption studies (56). However, the absorption and CD frequencies may not be identical, since the CD spectrum is due to an electronic mechanism whereas the absorption spectrum is due to a vibronic mechanism. This greater magnitude of splitting is also in agreement with the conclusions of Russell and Douglas (57) based on CD and magnetic circular dichroism (MCD) studies. Also, the parallel between the nmr results and the Gaussian resolutions of the CD spectra indicated that the greater the distortion along the C_3 axis, the greater the trigonal splitting. Thus, the intensities observed in the experimental CD curves are probably much closer to the actual intensities than was previously assumed.

Beddoe and Mason (58) and Gollogly and Hawkins (59) recently assigned the high energy component of the CD curve of $\Lambda[Co(tn)_3]^{+++}$ to the $^1A_1 \rightarrow {}^1A_2$ transition. This assignment was made on the basis of the criterion of Mason *et al.* (60,61) that the intensity of the A_2 band is increased at the expense of the E_a band when highly-charged oxyanions are added to a solution of the complex ion. The single crystal CD spectrum of $\Delta[Co(tn)_3]Cl_3 \cdot 4H_2O$ reported herein and elsewhere (62) does not agree with this assignment. As previously mentioned, light propagation was parallel to the C_3 axis of the complex ion (within experimental error) and thus the spectrum should be due to the $^1A_1 \rightarrow {}^1E_a$ transition only. This spectrum (see Figure 10) indicates that the high energy band is the E_a band and not the A_2 band.

From the experimental results presented in this thesis, it may be concluded that the prediction by Piper (63) that the signs of the

Cotton effects will reverse with respect to the ethylenediamine complex if the N-Co-N angle within a chelate ring is greater than 90° is correct. Or perhaps more accurately, it may be concluded that Piper and Karipides' (12) prediction of a change in sign of the Cotton effects with a change in sign of the azimuthal distortion is correct. Perhaps the most important conclusion is that Karipides and Piper's (15) predictions on the basis of their molecular orbital model are correct. It should be noted that these conclusions are based on only very few experiments, and clearly more experiments need to be performed on compounds in which the chelate ring angle is greater than 90°.

It appears that it is not safe to assume that molecules with the same signs of the rotational strengths of their component bands have the same absolute configuration unless the first coordination spheres of the complexes are virtually identical. Thus, it appears to be safe to infer the absolute configuration of $\Lambda[Co(d\text{-pn})_3]^{+++}$ from that of $\Lambda[Co(en)_3]^{+++}$. However, as was shown here, this correlation may not be extended to $\Delta[Co(tn)_3]^{+++}$.

The empirical rule of relating the sign of the long wavelength CD band in the visible region and the absolute configuration was found to hold in the cases presented here. To establish the validity of this rule, more experiments must be done to determine absolute configurations of complex ions.

The ORD and CD curves of $\Lambda[Co(d\text{-pn})_3]^{+++}$ closely resemble those of $\Lambda[Co(en)_3]^{+++}$. It has been supposed (52) that the component bands of the CD spectrum of $\Lambda[Co(d\text{-pn})_3]^{+++}$ could be assigned in the same way as those of $\Lambda[Co(en)_3]^{+++}$. This supposition was in agreement with the re-

sults of this work. The single crystal CD spectrum of $\Lambda[Co(d\text{-pn})_3]Br_3$ indicated a long wavelength, positive rotational strength, E_a component, the same as for the $\Lambda[Co(en)_3]^{+++}$ ion. As was pointed out by Saito (52), this was the first proven case of the usefulness and reliability of the conventional method of correlating the absolute configurations with the ORD curves.

To summarize, the results of this work suggest the following tentative generalizations about the *tris*-bidentate cobalt(III) complexes.

1. The separation of the A_2 and E_a components in the CD spectrum is greater than would be indicated by the absorption spectrum and is directly proportional to the polar distortion of the complex along the C_3 axis, with a compression giving a negative value to the trigonal splitting ($\nu_E - \nu_A < 0$) and an elongation giving a positive splitting. The electronic distortion at the Co(III) ion and the geometrical distortion of the ligand atoms are directly related and so the "orbital mismatch" in the sense used by Liehr seems to be small. This suggestion is based on a comparison of the magnitudes of the quadrupole coupling constants of ^{59}Co in the ions studied here and those of ^{51}V in some tetrahedral vanadium compounds (64). Although this comparison may not be direct, the coupling constants of ^{59}Co obtained here are of the same order of magnitude as those of the vanadium compounds. The quadrupole coupling constants for the vanadium compounds are apparently due to small deviations from tetrahedral symmetry. Thus, the magnitudes of the coupling constants for ^{59}Co are of the order expected for the relatively small distortions.

2. The signs of the rotational strengths associated with the

A_2 and E_a components are of opposite sign and the signs are determined by the sign of the azimuthal distortion and not by the chirality of the complex. Also, the magnitudes of the rotational strengths are directly related to the magnitude of the azimuthal distortion. Namely, as the azimuthal distortion becomes greater, the rotational strength becomes greater.

3. The model of Karipides and Piper (15) gives correct qualitative predictions relating the distortions of the complex ions and the features of the CD curves. This applies to the ions reported herein, but more studies of the type reported here must be made to verify the predictions of the model for other compounds.

Little may be said at this time about the ion, $(+)_{589}[Co_2(trien)_3]^{6+}$ except to note that the ORD and CD curves for the ion are similar to those of $\Lambda[Co(en)_3]^{3+}$. Also, the nmr results indicated two unique cobalt sites in the crystal, $[Co_2(trien)_3](NO_3)_6 \cdot 6H_2O$.

X-Ray work needs to be done to determine if the structure of the ion as proposed by Busch (26) is correct. If the structure is that proposed by Busch, then a single crystal CD study of the optically active ion would be indicated. The identification of the component bands of the CD spectrum and the determination of the structure of this ion could help determine the correct theoretical model pertaining to optical activity.

REFERENCES*

1. J. B. Biot, *Mem. Inst.*, 1, 1 (1812).
2. J. B. Biot, *Mem. Acad. Sci.*, 13, 39 (1835).
3. J. B. Biot, *Mem. Acad. Sci.*, 15, 93 (1838).
4. A. Fresnel, *Ann. Chim. Phys.*, 28, 147 (1825).
5. W. Haidinger, *Ann. Phys.*, 70, 531 (1847).
6. A. Cotton, *Compt. Rend.*, 120, 989, 1044 (1895).
7. L. Orgel, *J. Chem. Phys.*, 23, 1004 (1955).
8. W. Kuhn and K. Bein, *Z. Phys. Chem., B*, 24, 335 (1934); *Z. Anorg. Chem.*, 216, 321 (1934).
9. L. L. Jones and H. Eyring, *J. Chem. Educ.*, 38, 601 (1961).
10. W. Moffitt, *J. Phys. Chem.*, 25, 1189 (1956).
11. N. K. Hamer, *Mol. Phys.*, 5, 339 (1962).
12. T. S. Piper and A. Karipides, *Mol. Phys.*, 5, 475 (1962).
13. H. Poulet, *J. Chim. Phys.*, 59, 584 (1962).
14. M. Shinada, *J. Phys. Soc. Jap.*, 19, 1607 (1964).
15. A. G. Karipides and T. S. Piper, *J. Chem. Phys.*, 40, 674 (1964).
16. A. D. Liehr, *J. Phys. Chem.*, 68, 665 (1964).
17. A. J. McCaffery and S. F. Mason, *Mol. Phys.*, 6, 359 (1963).
18. C. E. Schäffer, *Proc. Roy. Soc., Ser. A*, 297, 96 (1967).
19. K. Nakatsu, M. Shiro, Y. Saito, and H. Kuroya, *Bull. Chem. Soc. Jap.*, 30, 158 (1957).

---

*Literature refernces to technical journals follow the system of abbreviations as given in the *Chemical Abstracts List of Periodicals*, 50, 1 (1956).

20. K. Nakatsu, *Bull. Chem. Soc. Jap.*, 35, 832 (1962).

21. M. Iwata, K. Nakatsu, and Y. Saito, *Acta Cryst.*, *B*, 25, 2562 (1969).

22. H. Iwasaki and Y. Saito, *Bull. Chem. Soc. Jap.*, 39, 92 (1966).

23. T. Nomura, F. Marumo, and Y. Saito, *Bull. Chem. Soc. Jap.*, 42, 1016 (1969).

24. *Inorg. Chem.*, 9, 1 (1970).

25. F. Basolo, *J. Amer. Chem. Soc.*, 70, 2634 (1948).

26. D. H. Busch in "Cobalt, Its Chemistry, Metallurgy and Uses," ed. by R. S. Young, No. 149, Chap. 6, New York, Reinhold Publishing Corp., 1960.

27. L. Rosenfeld, *Z. Phys.*, 52, 161 (1928).

28. E. U. Condon, *Rev. Mod. Phys.*, 9, 432 (1937).

29. E. Hückel, *Z. Elektrochem.*, 50, 13 (1944).

30. W. Moffitt and A. Moscowitz, *J. Chem. Phys.*, 30, 648 (1959).

31. E. U. Condon, W. Altar, and H. Eyring, *J. Chem. Phys.*, 5, 753 (1937).

32. S. Sugano, *J. Chem. Phys.*, 33, 1883 (1960).

33. R. V. Pound, *Phys. Rev.*, 79, 685 (1950).

34. R. Bersohn, *J. Chem. Phys.*, 20, 1505 (1952).

35. G. M. Volkoff, H. E. Petch, and D. W. L. Smellie, *Can. J. Phys.*, 30, 270 (1952).

36. G. M. Volkoff, *Can. J. Phys.*, 31, 820 (1953).

37. L. C. Brown, Ph.D. Thesis, The Ohio State University, Columbus, Ohio, 1955.

38. H. M. Cohen and F. Reif, *Solid State Phys.*, 5, 321 (1957).

39. T. P. Das and E. L. Hahn, *Solid State Phys., Suppl. 1* (1958).

40. L. C. Brown and P. M. Parker, *Phys. Rev.*, 100, 1764 (1955).

41. B. A. Whitehouse, J. D. Ray, and D. J. Royer, *J. Mag. Res.*, 1, 311 (1969).

42. B. A. Whitehouse, Ph.D. Thesis, Georgia Institute of Technology, Atlanta, Georgia, 1967.

43. J. B. Work, "Inorganic Syntheses," 2, 221 (1946).

44. J. A. Broomhead, F. P. Dwyer, and J. W. Hogarth, "Inorganic Syntheses," 6, 186 (1960).

45. J. C. Bailar and J. B. Work, *J. Amer. Chem. Soc.*, 68, 232 (1946).

46. G. E. Ryschkewitsch and J. M. Garrett, *J. Amer. Chem. Soc.*, 90, 7234 (1968).

47. F. Woldbye, Final Technical Report to the European Research Office, U. S. Department of the Army, Frankfurt am Main, June 30, 1959, Contract No. DA-91-508-EUC-246.

48. F. Woldbye, *Rec. Chem. Progr.*, 24, 197 (1963).

49. F. P. Dwyer, F. L. Garvan, and A. Shulman, *J. Amer. Chem. Soc.*, 81, 290 (1959).

50. E. Drouard and J. P. Mathieu, *C. R. Acad. Sci., Paris*, 236, 2395 (1953).

51. V. H. Schievelbein, Ph.D. Thesis, Georgia Institute of Technology, Atlanta, Georgia, 1969.

52. Y. Saito, *Pure Appl. Chem.*, 17, 21 (1968).

53. F. Woldbye, *Proc. Roy. Soc., Ser. A*, 297, 79 (1967).

54. T. S. Piper and R. L. Carlin, *J. Chem. Phys.*, 35, 1809 (1961).

55. T. S. Piper and R. L. Carlin, *J. Chem. Phys.*, 36, 3330 (1962).

56. S. Yamada and R. Tsuchida, *Bull. Chem. Soc. Jap.*, 33, 98 (1960).

57. R. L. Russell and B. E. Douglas, *Inorg. Chim. Acta*, 3, 426 (1969).

58. P. G. Beddoe and S. F. Mason, *Inorg. Nucl. Chem. Lett.*, 4, 433 (1968).

59. J. R. Gollogly and C. J. Hawkins, *Chem. Commun.*, 689 (1968).

60. S. F. Mason and B. J. Norman, *Proc. Chem. Soc.*, 339 (1964).

61. R. Larsson, S. F. Mason, and B. J. Norman, *J. Chem. Soc., A*, 301 (1966).

62. R. R. Judkins and D. J. Royer, *Inorg. Nucl. Chem. Lett.*, In Press.

63. T. S. Piper, *J. Amer. Chem. Soc.*, 83, 3908 (1961).

64. V. Saraswati, *J. Phys. Soc. Jap.*, 23, 761 (1967).

VITA

Roddie Reagan Judkins was born December 31, 1941 in Sunbright, Tennessee to Ammon Eston and Hazel McAfee Judkins. He attended high school at Sunbright High School in Sunbright, Tennessee and was graduated in May, 1959. He attended Tennessee Polytechnic Institute in Cookeville, Tennessee and received a Bachelor of Science in Engineering Chemistry degree in June, 1963. In June, 1965, he received a Master of Science degree in Chemistry from Tennessee Polytechnic Institute.

In September, 1965, he entered Georgia Institute of Technology in Atlanta, Georgia. He was employed as an instructor in chemistry for the School of Chemistry at the Georgia Institute of Technology during the course of his graduate study.

He held the faculty awarded Du Pont Teaching Assistant Fellowship for two quarters. He was elected to the Society of the Sigma Xi in June, 1969.

He is married to the former Teressa Dean Ward of Sunbright, Tennessee. They are the parents of two daughters, Bridget Renee and Lisa Suzanne.